Monthly Notices
of the
ROYAL ASTRONOMICAL SOCIETY

MNRAS **478,** 228–254 (2018)
Advance Access publication 2018 April 05

doi:10.1093/mnras/sty865

The GALAH survey: stellar streams and how stellar velocity distributions vary with Galactic longitude, hemisphere, and metallicity

Alice C. Quillen,[1★†] Gayandhi De Silva,[2,3] Sanjib Sharma,[3] Michael Hayden,[3,4] Ken Freeman,[5] Joss Bland-Hawthorn,[3,4,6] Maruša Žerjal,[5] Martin Asplund,[4,5] Sven Buder,[7] Valentina D'Orazi,[8] Ly Duong,[5] Janez Kos,[3] Jane Lin,[5] Karin Lind,[7,9] Sarah Martell,[10] Katharine Schlesinger,[5] Jeffrey D. Simpson,[2] Daniel B. Zucker,[2,11,12] Tomaz Zwitter,[13] Borja Anguiano,[11,14] Daniela Carollo,[4,15] Luca Casagrande,[5] Klemen Cotar,[13] Peter L. Cottrell,[16,17] Michael Ireland,[5] Prajwal R. Kafle,[18] Jonathan Horner,[19] Geraint F. Lewis,[3] David M. Nataf,[20] Yuan-Sen Ting,[21,22,23] Fred Watson,[2] Rob Wittenmyer[24,25] and Rosemary Wyse[20]

Affiliations are listed at the end of the paper

Accepted 2018 April 3. Received 2018 February 8; in original form 2018 March 31

ABSTRACT

Using GALAH (GALactic Archaeology with HERMES) survey data of nearby stars, we look at how structure in the planar (u, v) velocity distribution depends on metallicity and on viewing direction within the Galaxy. In nearby stars with distance $d \lesssim 1$ kpc, the Hercules stream is most strongly seen in higher metallicity stars [Fe/H] > 0.2. The Hercules stream peak v value depends on viewed galactic longitude, which we interpret as due to the gap between the stellar stream and more circular orbits being associated with a specific angular momentum value of about 1640 km s^{-1} kpc. The association of the gap with a particular angular momentum value supports a bar resonant model for the Hercules stream. Moving groups previously identified in *Hipparcos* (HIgh Precision Parallax COllecting Satellite) observations are easiest to see in stars nearer than 250 pc, and their visibility and peak velocities in the velocity distributions depends on both viewing direction (galactic longitude and hemisphere) and metallicity. We infer that there is fine structure in local velocity distributions that varies over distances of a few hundred pc in the Galaxy.

Key words: Galaxy: disc – Galaxy: evolution – Galaxy: kinematics and dynamics.

1 INTRODUCTION

Stars in the disc of the Milky Way can be described in terms of their distributions in space, velocity, age, and chemical abundances. Star formation takes place in gas structures producing young compact clusters, moving groups and stellar associations that evaporate, disrupt, and are dispersed across the Galaxy, while leaving imprints in velocity and chemical abundance distributions (Eggen 1958a,b,c, 1965a,b,c, 1970, 1995, 1996, 1998; Freeman & Bland-Hawthorn 2002; Baumgardt & Makino 2003; De Silva et al. 2007). Non-axisymmetric perturbations from spiral arms, a bar or satellite galaxies can also induce gaps, overdensities, or dynamical streams (Kalnajs 1991; Weinberg 1994; Dehnen 1999b, 2000; Fux 2001; Quillen 2003; Quillen & Minchev 2005; Chakrabarty & Sideris 2008; Quillen et al. 2009; Gardner & Flynn 2010; Minchev et al. 2010; Lepine et al. 2011; Quillen et al. 2011; Grand et al. 2015) that can be seen in *local* velocity distributions that are constructed from stars restricted to small regions or neighbourhoods in the Galaxy.

Because streams and clumps are seen in the velocity distribution of stars in the solar neighbourhood (Kapteyn 1905; Dehnen 1998; Skuljan, Hearnshaw & Cottrell 1999; Famaey et al. 2005), this distribution is poorly described by a single velocity ellipsoid (Schwarzschild 1907; Robin et al. 2017; Anguiano et al. 2018). If clumps or gaps in the velocity distribution of old stars in the disc are due solely to resonances with spiral or bar patterns (e.g. Kalnajs 1991; Dehnen 2000; Fux 2001; Quillen & Minchev 2005), then we would expect those clumps and gaps to only be seen in

★ E-mail: alice.quillen@gmail.com
† Simons Fellow in Theoretical Physics.

specific neighbourhoods where the resonant perturbations are strongest, rather than throughout the disc. In contrast, if clumps in the velocity distribution are primarily due to dissolution of star clusters then they would predominantly be comprised of homogeneous (in abundances and age) groups of stars (Eggen 1958a; Freeman & Bland-Hawthorn 2002; De Silva et al. 2007; Bland-Hawthorn, Krumholz & Freeman 2010). The extent of structure in local velocity distributions outside the solar neighbourhood is not yet known, though dissection of test particle and *N*-body simulations suggests that local velocity distributions could exhibit substructures such as gaps and clumps all over the Galaxy (De Simone, Wu & Tremaine 2004; Quillen et al. 2011; Grand et al. 2015).

As the number of stars with accurate proper motions, radial velocities, and parallaxes increases with ongoing surveys, we can attempt to break the degeneracies between models for the different dynamical mechanisms by studying variations in the local velocity distributions as a function of position in the Galaxy or distance from the Sun. The Radial Velocity Experiment (RAVE; Steinmetz et al. 2006), the Large Sky Area Multi-Object Fibre Spectroscopic Telescope (LAMOST; Zhao et al. 2012) survey, The Geneva Copenhagen survey (Holmberg, Nordström & Andersen 2009), the GAIA-ESO survey (Gilmore et al. 2012; Randich et al. 2013), the US Naval Observatory CCD Astrograph Catalog 5 (UCAC5; Zacharias, Finch & Frouard 2017), the Sloan Extension for Galactic Understanding and Exploration survey (SEGUE; Yanny et al. 2009), and the Apache Point Observatory Galactic Evolution Experiment (APOGEE; Majewski et al. 2015) are surveys that have increased the number and distance of stars from the Sun with kinematic measurements compared to the HIgh Precision Parallax COllecting Satellite (*Hipparcos*) catalogue (Perryman et al. 1997) which primarily contains nearby stars less than 100 pc away (Dehnen 1998; Famaey et al. 2005). The increased distances have made it possible to search for radial and vertical gradients in mean velocities measured from local velocity distributions (Siebert et al. 2011; Carlin et al. 2013; Williams et al. 2013; Sun et al. 2015; Xu et al. 2015; Pearl et al. 2017; Carrillo et al. 2018). One feature that is seen to vary as a function of position in the Galaxy is that associated with the feature known as the *U-anomaly* or Hercules stream (Antoja et al. 2014; Monari et al. 2017; Perez-Villegas et al. 2017). Hyades and Sirius streams were identified in K giants up to 1.5 kpc from the Sun (Wilson 1990).

Fibre-fed spectroscopic surveys continue to expand on the number and accuracy of measurements of stars in the Galaxy. Here, we focus on kinematic and abundance measurements of half a million stars from the GALactic Archaeology with HERMES (GALAH) survey. Our focus is searching for variations in substructure in local velocity distributions near the Sun. From GALAH survey data, we construct velocity distributions from stars in angular regions defined by their viewed galactic longitude. This gives us velocity distributions in local neighbourhoods that are displaced by a few hundred pc from the location of the Sun in the Galaxy. In Section 3, we examine how velocity distributions vary as a function of viewed galactic longitude and we use GALAH's spectroscopic measurements to see how these velocity distributions depend on metallicity. In Section 4, we examine the Hercules stream. In Section 5, we examine clumps in the velocity distribution in nearby samples of GALAH stars to see how low-velocity streams vary with position near the Sun.

2 GALAH SPECTROSCOPIC SURVEY OF THE GALAXY

The GALAH survey[1] (De Silva et al. 2015; Kos et al. 2017, 2018; Martell et al. 2017; Duong et al. 2018) is a large observing programme using the High Efficiency and Resolution Multi-Element Spectrograph (HERMES; Sheinis et al. 2015) with the 3.9 m Anglo-Australian Telescope of the Australian Astronomical Observatory. Light is directed into HERMES from the 2dF multiple-fibre positioner (Lewis et al. 2002), so spectra of up to 392 stars can be obtained simultaneously. GALAH is a high-resolution ($R = 28\,000$) stellar spectroscopic survey of approximately a million stars, exploring the chemical and dynamical history of the Milky Way (De Silva et al. 2015) that measures radial velocities and stellar abundances for as many as 30 elements (Kos et al. 2017).

Spectroscopic measurements for the GALAH survey spectra are done with a data-driven approach, using the *Cannon*, giving effective temperature, effective surface gravity, and abundance measurements from the stellar spectra (Ness et al. 2015; and see section 2 by Sharma et al. 2018). For more details on the GALAH data reduction pipeline and derived measurements, see Kos et al. (2017), Martell et al. (2017), and Sharma et al. (2018). HERMES with 2dF and the same data reduction and measurement pipelines are also used to characterize stellar targets for The Transiting Exoplanet Survey Satellite (TESS) (the TESS-HERMES programme; Sharma et al. 2018) and for spectroscopic follow-up of *Kepler* Satellite K2 fields (the K2-HERMES programme; Wittenmyer et al. 2018).

The GALAH input catalogue stars are selected using near-infrared 2-Micron All-Sky Survey (2MASS; Skrutskie et al. 2006) *JHK* photometry of stars to estimate *V*-band magnitudes using the conversion: $V(J, K) = K + 2(J - K + 0.14) + 0.382 \exp((J - K - 0.2)/0.5)$ (following section 5.1 by De Silva et al. 2015). From these estimated *V*-band magnitudes, stars with the *V* band in the range of 12–14 mag are selected for observation. Stars are restricted to galactic latitudes $|b| > 10^\circ$ and declinations $-80^\circ <$ Dec. $< +10^\circ$. For more information about GALAH target selection, see section 5.1 by De Silva et al. (2015) and Martell et al. (2017). The TESS-HERMES programme target stars are also restricted in magnitude but with *V* band between 10 and 13.1 mag. As a result, that programme contains brighter stars than the GALAH survey. The K2-HERMES programme extends to a fainter *V* mag of 15 and is restricted to redder stars with $J - K > 0.5$.

The GALAH observed sample contains few previously known cluster stars (see table 2 and discussion by Kos et al. 2018 and Martell et al. 2017), though open and globular clusters have been observed with supplemental observational programmes [K2-HERMES, the cluster and pilot programmes (De Silva in preparation; Duong et al. 2018; Wittenmyer et al. 2018)]. We attribute the lack of cluster stars in the GALAH survey to logistics associated with fibre positioning (nearby targets on the sky cannot be observed simultaneously) and scheduling of fields containing higher densities of stars.

The spectroscopic parameters and abundances used here are those from GALAH internal data release 2 (iDR2) using *Cannon* version 2.7 (Buder et al. in preparation); however, Bayesian inferred estimates for distance and age are those from *Cannon* version 1.3 and as described by Sharma et al. (2018) in their section 3. The differences in stellar parameters are minimal between the two data releases. The main difference is that more detailed abundances are available

[1] http://galah-survey.org

in iDR2 and for a larger sample of stars. The number of stars in the data table that we are using is 539594.

We use positions and proper motions from the US Naval Observatory CCD Astrograph Catalog 5 (UCAC5) (Zacharias et al. 2017), where the precision level of the *Tycho–Gaia* Astrometric Solution (TGAS) proper motions (Michalik, Lindegren & Hobbs 2015) is extended to many millions more stars.

The *Gaia*-ESO Survey (Gilmore et al. 2012; Randich et al. 2013) contains a sample of about 100000 stars over 14–19 in *V* band, most of which are thick disc and halo stars, as well as specially targeted star clusters. In contrast, GALAH has more stars, a narrower magnitude range, lacks star clusters, and contains more dwarf and thin disc stars. The near-infrared APOGEE survey targeted the plane of the disc with a sample of 150000 red giants. As the survey targets giants, APOGEE stars tend to be more distant than GALAH stars. The APOGEE-S survey is carrying out a survey of similar design and scale from the Southern hemisphere. The magnitude ranges and different regions of the Galaxy covered make both *Gaia*-ESO and APOGEE are complementary to the GALAH sample, with minimal overlap. The RAVE survey (Steinmetz et al. 2006) contains a similar number of stars as the current GALAH sample and there is some overlap with GALAH. The RAVE sample spanning magnitudes from 8 to 12 in the *I* band were selected from multiple input sources over the time span of the survey and includes a colour selection of $J - K$ mag >0.5 so it preferentially selects giants (see Wojno et al. 2017). In contrast, the GALAH sample is sourced solely from 2MASS photometry, has a well-defined selection function, and when compared to RAVE, is dominated by local disc dwarfs making it more sensitive to nearby substructure in the Galaxy.

2.1 Coordinates

To discuss the velocity distribution of stars in the Galactic disc, we first define a Galactic coordinate system. We adopt a Cartesian galactocentric coordinate system with origin at the Galactic Centre and the Sun at $(x_\odot, y_\odot, z_\odot) = (-\mathrm{R}_\odot, 0, 0)$, where $\mathrm{R}_\odot$ is the galactocentric radius of the Sun. We ignore the offset of the Sun from the Galactic plane ($z_\odot = 25 \pm 5$ pc; Bland-Hawthorn & Gerhard 2016). In a cylindrical coordinate system (r, θ, z), the velocity of a star has radial, tangential, and vertical components (v_r, v_θ, v_z). The local standard of rest (LSR) corresponds to a circular orbit at a radius $\mathrm{R}_\odot$, in the Galactic plane, with $v_r = v_z = 0$ and $v_\theta = -V_{\mathrm{circ},\odot}$. The velocity $V_{\mathrm{circ},\odot}$ is the speed of a star in a circular orbit at the Sun's radius (ignoring non-axisymmetric perturbations by spiral arms or the Galactic bar).

By a common convention, the velocity components $(u, v, w) = (-v_r, -v_\theta - V_{\mathrm{circ},\odot}, v_z)$ are velocities in cylindrical coordinates subtracted from the local standard of rest, with u equal to minus 1 times the radial velocity component, and with large positive v for stars at high angular momentum coming from the outer Galaxy into the solar neighbourhood. The negative sign for v_θ gives a Cartesian coordinate system for Galactic rotation with positive z towards the north Galactic pole.

In the inertial Galactic coordinate system, we adopt space motions for the Sun $v_{\theta,\odot} = -242.0\,\mathrm{km\,s^{-1}}$, $v_{r,\odot} = 11.1\,\mathrm{km\,s^{-1}}$, and $v_{z,\odot} = 7.25\,\mathrm{km\,s^{-1}}$. The galactocentric radius of the Sun $\mathrm{R}_\odot = 8.0$ kpc is that by Reid (1993; see Sharma et al. 2014, section 2.5) for discussion regarding this choice. The radial and vertical peculiar space motions of the Sun (with respect to LSR) $v_{r,\odot}$ and $v_{z,\odot}$ are by Schönrich, Binney & Dehnen (2010). The tangential space motion of the Sun $-v_{\theta,\odot} = V_{\mathrm{circ},\odot} + v_{\odot,\mathrm{pec}}$ is observationally well constrained by the angular rotation rate of Sgr A* ($30.24\,\mathrm{km\,s^{-1}\,kpc^{-1}}$; Reid & Brunthaler 2004; see Sharma et al. 2014, section 6.3). For $\mathrm{R}_\odot = 8.0$ kpc, the angular rotation rate of Sgr A* gives a tangential velocity $-v_{\theta,\odot} = 30.24 \times 8.0 = 241.92\,\mathrm{km\,s^{-1}}$, consistent with the adopted value given above and used to compute v_θ for each star. Here, $v_{\odot,\mathrm{pec}}$ is the Sun's peculiar velocity with respect to the LSR. For $v_{\odot,\mathrm{pec}} \approx 10\,\mathrm{km\,s^{-1}}$ (as found by Schönrich et al. 2010) the circular velocity at the galactocentric radius of the Sun $V_{\mathrm{circ},\odot} \approx 230\,\mathrm{km\,s^{-1}}$ (see section 5.3.3 by Bland-Hawthorn & Gerhard 2016).

From positions, proper motions, and distances, GALAH spectroscopically measured radial velocities and using the Sun's space motion (as described above) the galactocentric cylindrical coordinates are computed for each star in the survey $[\theta, r, z, v_\theta, v_r, v_z]$. From these and using $V_{\mathrm{circ},\odot} = 230\,\mathrm{km\,s^{-1}}$ we compute velocity components (u, v, w). Our choice for $V_{\mathrm{circ},\odot}$ is $30\,\mathrm{km\,s^{-1}}$ higher than used by Dehnen (1998) (who adopted $V_{\mathrm{circ},\odot} = 200\,\mathrm{km\,s^{-1}}$, a somewhat lower $v_{\odot,\mathrm{pec}} = 5.2\,\mathrm{km\,s^{-1}}$ for the Sun and the same $\mathrm{R}_\odot = 8$ kpc). As a consequence, our v values for clumps identified in the velocity distributions are consistent with but $20–30\,\mathrm{km\,s^{-1}}$ lower than those reported by Dehnen (1998).

3 VELOCITY DISTRIBUTIONS CONSTRUCTED FROM STARS AT DIFFERENT GALACTIC LONGITUDES

To study local velocity distributions we construct histograms in radial and tangential velocity bins that are $4\,\mathrm{km\ s^{-1}}$ square. The numbers of stars in each bin gives the distribution of stars as a function of the two in-plane velocity components. We construct velocity distributions from stars in different angular regions in galactic longitude. Central galactic longitudes for each region range between $\ell = 180°$ (the Galactic anticentre direction) and $\ell = 40°$, in steps of 20°, and covering the Galactic Centre direction at $\ell = 0°$. We neglect the region between $\ell = 40°$ and $\ell = 180°$. It is not well sampled because the GALAH survey has few stars in this direction on the sky. Each region is $\Delta\ell = 40°$ wide in galactic longitude, so the neighbourhoods we use to construct histograms overlap each other. For example, the histogram centred at $\ell = 260°$ is constructed from stars with $240° < \ell < 280°$. We eliminate stars with high or low galactic latitudes, $|b| > 45°$, and stars with distance errors $\sigma_d/d > 0.5$, where d is the distance and σ_d its computed error (standard deviation; see section 3 by Sharma et al. 2018). For stars with $d < 1$ kpc, 500 pc, or 250 pc, the median values of σ_d/d are 0.23, 0.18, and 0.14. Table C1 lists the cuts made to the survey stars relevant for each figure and table in this manuscript.

We also eliminate stars observed as part of dedicated observing programmes of open clusters (De Silva in preparation) and GALAH pilot surveys (Duong et al. 2018); however, we did not remove stars observed as part of the K2-HERMES (Wittenmyer et al. 2018) or TESS-HERMES (Sharma et al. 2018) observing programmes because they increase the number of stars observed near the Galactic anticentre. We have checked that removal of the K2-HERMES and TESS-HERMES programme stars does not impact the appearance of the histograms. After excluding those with large distance errors, which are part of open cluster observing programmes or have $|b| > 45°$, the number of GALAH survey stars remaining in iDR2 is 376510. Within this group, the number of stars observed as part of K2-HERMES and TESS-HERMES programmes is 69162.

Each histogram is constructed from stars within a specific metallicity range and a specific range in estimated distance. Because each histogram is constructed from a distance limited sample and only

along a particular viewing direction, the median position in galactic (x, y) coordinates of the stars is not at the position of the Sun. Thus, each histogram gives a velocity distribution constructed from stars in different local neighbourhoods.

Fig. 1 shows four sets of histograms, each constructed only of stars within $d < 500$ pc. Fig. 1(a) (top panel) shows metal-rich stars with [Fe/H] > 0.2, Fig. 1(b) (the second from the top panel) shows near solar metallicity stars with $-0.1 <$ [Fe/H] < 0.2, Fig. 1(c) (the third from the top panel) shows lower metallicity stars with [Fe/H] < -0.1, and Fig. 1(d) (bottom panel) shows high-α-element (thick disc) stars with [α/Fe] > 0.2. The distance limit eliminates giants due to the magnitude limit of the GALAH survey and we have checked that removal of stars with stellar surface gravity $\log g < 3.5$ does not affect the appearance of the distributions. Each histogram has x-axis showing the radial velocities $u = -v_r$ of the velocity bins and y-axis the tangential velocities $v = -v_\theta - 230\,\mathrm{km\,s^{-1}}$ of the velocity bins. Each panel in a row is for stars restricted to within 20° of a particular galactic longitude with central galactic longitude beginning at $\ell = 180°$, on the left, and increasing in 20° steps to the right. The central galactic longitudes are labelled on the top of each histogram and the number of stars used to make each histogram is labelled on the bottom.

The histograms are normalized so that they integrate to 1 and are displayed with the same colourbar. The numbers on the colourbar show normalized counts in each bin. Specifically the numbers shown on the colourbar are the number of stars in the bin divided by the bin area (16 (km s^{-1})^2) divided by the number of stars in the histogram. The number of stars in each histogram impacts the precision of the velocity distribution. Histograms with few stars exhibit clumps that are due solely to the small numbers of stars in each bin. For reference, the panel of Fig. 1(a) at $\ell = 200°$ has about 1000 stars. Its peak 4 km s^{-1} square bin contains 12 stars and has a value of 0.0007 in the normalized histogram (and corresponding to the numbers shown on the colourbar). In the same histogram, the dark green contours have only a couple of stars per bin.

We consider how measurement errors in radial velocity and proper motions affect the (u, v) errors at different galactic longitudes. Because we have discarded high and low galactic latitude stars we can neglect galactic latitude for this discussion. At a viewing angle with galactic longitude $\ell = 270°$, the v velocity component is determined by the radial or line-of-sight velocity and the u velocity component is determined by the proper motions. At a galactic longitude of $\ell = 0°$or 180°, the opposite is true; the v velocity component is determined by the proper motions and the u velocity component is set by the radial velocity. Thus, the errors in (u, v) form an ellipse that is dependent on viewing direction.

Line-of-sight (radial) velocity component errors (standard deviations) from the GALAH data reduction pipeline are currently about $\sigma_{v\mathrm{los}} \approx 1\,\mathrm{km\,s^{-1}}$ (see Kos et al. 2017 and Fig. 6 by Sharma et al. 2018).[2] The tangential velocity component of a star $v_{\mathrm{tan}} = \mu\, d$, where d is the distance from the Sun and μ is the proper motion. For each star with error in distance ratio $\sigma_d/d < 0.5$ (as those are used to make our histograms), we estimate the error in the tangential velocity component $\sigma_{v\mathrm{tan}}$ from the distance d, distance error σ_d, the UCAC5 proper motion μ, and its error σ_μ:

$$\left(\frac{\sigma_{v\mathrm{tan}}}{v_{\mathrm{tan}}}\right)^2 = \left(\frac{\sigma_d}{d}\right)^2 + \left(\frac{\sigma_\mu}{\mu}\right)^2. \quad (1)$$

[2]Ongoing improvements in the data reduction pipeline are expected to decrease the error to ~ 0.1 km s^{-1} (Janez Kos, private communication).

We find a median error in the tangential velocity component of $\sigma_{v\mathrm{tan}} \approx 1.2$ and 1.8 km s^{-1} for stars with distances within 0.5 and 1 kpc, and 2.7 km s^{-1} for stars at all distances. As the error for the nearer stars is similar to that of the line-of-sight velocity component, $\sigma_{v\mathrm{tan}} \sim \sigma_{v\mathrm{los}}$, there is no strong directional dependence (dependence on galactic longitude) to the u and v velocity component errors. The size of the estimated tangential velocity errors are small enough that they would not have obscured structure smaller than a few km s^{-1} in our histograms. Thus, variations in the numbers of clumps in the velocity distributions with galactic longitude is not caused by a difference in the sizes of errors in u compared to v that is sensitive to direction on the sky.

Some stars in iDR2 are binaries and their radial velocities may include binary reflex motions (e.g. Badenes et al. 2018; El-Badry et al. 2018). Using multiple epoch APOGEE observations, Badenes et al. (2018) found that 5.5 per cent of main sequence or subgiant stars (see their table 1) exhibited a change in measured radial velocity (between epochs) greater than 10 km s^{-1}. Binaries would blur or smooth the velocity distributions, adding faint wings on to high-density peaks. Our histograms are essentially an underlying velocity distribution convolved or smoothed with an error function that depends on the distribution of binary star motions. However, this blurring should not obscure strong peaks in the velocity distribution as only 5–10 per cent of the stars are affected (with ∼10 per cent of stars with variation in radial velocity greater than 1 km s^{-1}, estimated assuming a similar fraction of binary stars per decade in log semimajor axis). Though they may be included in GALAH DR2, repeat observations (spectra taken at different epochs) of GALAH survey stars are not present in our data table.

A clear chemical separation in the [α/Fe] versus [Fe/H] abundance plane can be made between thin and thick disc populations (see e.g. Bensby et al. 2007b; Adibekyan et al. 2012; Bensby, Feltzing & Oey 2014; Hayden et al. 2015). The *Cannon*'s [α/Fe] is an error-weighted mean of O, Mg, Si, Ca, and Ti abundance measurements (Buder et al. 2018; Buder et al. in preparation). Because the Ti measurements are the most precise, the [α/Fe] measurement is most strongly influenced by the Ti abundance. We chose [α/Fe] > 0.2 for Fig. 1(d) so as to exclude the α-element-pooror thin-disc stellar population, leaving primarily stars from the older α-element-richand thicker disc. See Fuhrmann (1998), Bensby, Feltzing & Lundstrom (2003), Bensby et al. (2014), and Duong et al. (2018) for discussion on the divisions between the two populations. The current GALAH pipeline mis-classifies some cool giants as dwarfs, giving a spurious excess of nearby high-α stars in the distance distribution. To minimize this contribution, we also removed stars with effective temperature below 4500° to make the bottom panel of Fig. 1. The distance distribution used to make the velocity distribution of Fig. 1 (bottom panel) is shown in Appendix B. The median error in [α/Fe] reported by the *Cannon* software for the $d < 500$ pc stars is 0.06.

The median error is similar for the [Fe/H] abundance; the reported error is 0.054 according to fig. 6 by Sharma et al. (2018) comparing the *Cannon* measurements to those in the training set.

We estimate the location of the neighbourhoods of our histograms based on the mean distances of the stars in each neighbourhood from the Sun. The median distances for the $d < 500$ pc sets are d_n= 340, 330, 330, and 320 pc (from the Sun) for the metal-rich, solar, metal-poor, and high-α groups of stars, respectively, shown in the histograms of Fig. 1. See Appendix B for complete distributions of distances for stars in each metallicity range. We have checked histograms in bins of v and d made for stars seen in different galactic longitudes and sets of histograms in bins of u and d. Neither set showed sensitivity of the distance distributions on direction, though

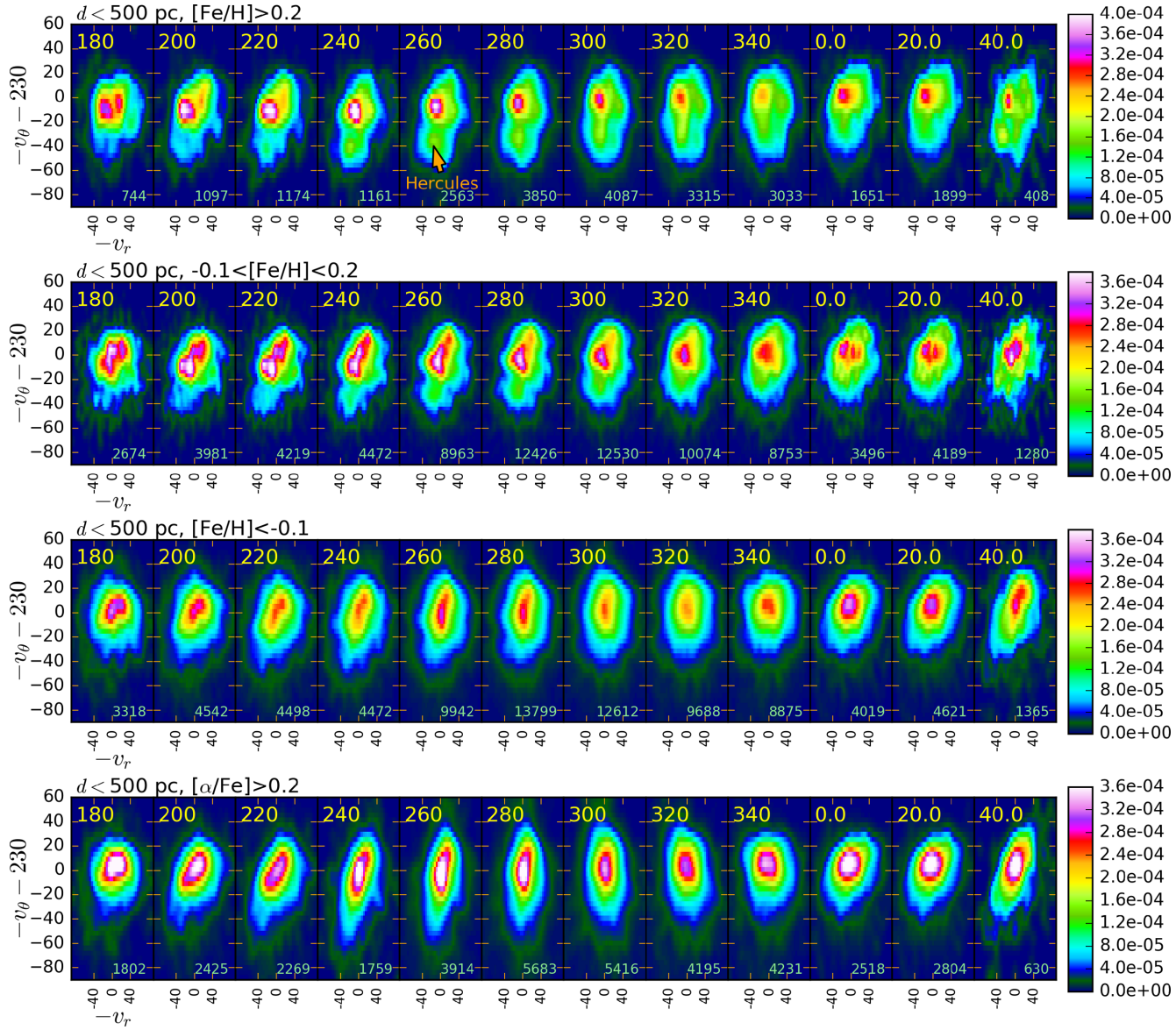

Figure 1. Histograms showing uv velocity distributions constructed of stars viewed at different galactic longitudes. The x-axes show the radial velocities $u = -v_r$ of each bin in km s^{-1}. The y-axes show the tangential velocities $v = -v_\theta - 230$ km s^{-1} of each bin in km s^{-1}. The histograms only contain nearby stars with distances $d < 500$ pc. The central galactic longitude for each histogram is the yellow number on the top of each histogram and the number of stars used to construct the histogram shown on the bottom. Each histogram is created using stars within 20° of the central galactic longitude. Each row of histograms is for stars within a different metallicity range. From top panel to bottom panel: (a) [Fe/H] > 0.2. (b) −0.1 < [Fe/H] < 0.2. (c) [Fe/H] < −0.1. (d) [α/Fe] > 0.2.

we re-examine this issue in Section 5.2 when we compare velocity distributions from stars in the northern Galactic hemisphere to that in the south.

4 THE HERCULES STREAM

The (u, v) velocity distributions for metal-rich stars shown in Fig. 1(a) exhibit an extension to lower tangential velocities v at about $v \sim -45$ km s^{-1} known as the Hercules stream. The stream is annotated in the galactic longitude $l = 260°$ histogram with an orange arrow in Fig. 1(a) (top panel). The Hercules stream (also called the U-anomaly) is one of the most prominent streams or clumps seen in the velocity distribution of stars in the solar neighbourhood (Eggen 1958b, 1965c; Dehnen 1998; Famaey et al. 2005; Ramya et al. 2016). The Hercules stream is seen as a separate feature because it is separated by a dip or gap in the numbers of stars at $v \sim -30$ km s^{-1} from stars in more nearly circular orbits at $v \sim 0$. The stream is centred at a negative radial velocity component $u \sim -20$ km s^{-1} corresponding to stars moving away from the Galactic Centre.

Stars in the Hercules stream span a range of ages and metallicities (e.g. Dehnen 1998; Famaey et al. 2005; Bensby et al. 2007a; Bovy & Hogg 2010; Ramya et al. 2016) implying that the division in phase space has a dynamical origin. The Hercules stream is thought to be caused by perturbations from the Galactic bar (Dehnen 1999b, 2000; Fux 2001; Minchev et al. 2010; Antoja et al. 2014; Monari et al. 2017; Perez-Villegas et al. 2017; Portail et al. 2017a). For a short and quickly rotating or *fast* bar, the Hercules stream is related to the bar's outer Lindblad resonance (Kalnajs 1991; Dehnen 2000; Minchev, Nordhaus & Quillen 2007; Antoja et al. 2014; Monari et al.

2017; Hunt et al. 2018). Stars in nearly circular orbits are outside this resonance and have orbits preferentially elongated parallel to the bar. Stars in the Hercules stream are inside resonance and in some models they are elongated perpendicular to the bar (Kalnajs 1991; Dehnen 2000; Fux 2001; Minchev et al. 2010), with two radial epicyclic oscillations per orbit in the bar's rotating frame. For a longer and slower bar, the stream is caused by orbits associated with a stable Lagrange point in the bar's corotation region (Perez-Villegas et al. 2017; Portail et al. 2017a). The galactocentric radius of corotation is that where the bar angular rotation rate or pattern speed is equal to the orbital angular rotation rate of a star in a circular orbit in a galaxy with the same azimuthally averaged mass distribution and lacking the bar. A fast rotating bar has pattern speed $\Omega_b = (1.89 \pm 0.08)\Omega_\odot$ or $\Omega_b = 56 \pm 2\,\mathrm{km\,s^{-1}\,kpc^{-1}}$ for a solar angular rotation rate $\Omega_\odot = 29.5\,\mathrm{km\,s^{-1}\,kpc^{-1}}$ (Antoja et al. 2014). For the *slow* bar, $\Omega_b = 39 \pm 2\,\mathrm{km\,s^{-1}\,kpc^{-1}}$ (Perez-Villegas et al. 2017; Portail et al. 2017a). *N*-body simulations show that spiral structure may influence the appearance of the Hercules stream in velocity distributions (Quillen et al. 2011; Grand et al. 2015).

Recent studies have shown that the visibility or contrast of the Hercules stream in the (u, v) or (v_r, v_θ) velocity distribution of stars in the solar neighbourhood is dependent on metallicity (Liu et al. 2015; Liu 2016; Perez-Villegas et al. 2017), with higher metallicity stars more clearly showing the gap separating the stream from the more nearly circular orbits at low $|u|$, $|v|$ (see fig. 5 by Perez-Villegas et al. 2017). The stream is predicted to be most easily detected in the velocity distribution for giant stars that are within 3 kpc from the Sun and observed near a galactic longitude of approximately 270° (Hunt et al. 2018). We confirm both of these trends. Fig. 1(a) (top panel) shows that the stream is most prominent at galactic longitudes $220° < \ell < 340°$ but is also weakly seen at $\ell \sim 40°$. A comparison of Fig. 1(a) (top panel), for higher metallicity stars with [Fe/H] > 0.2, with Fig. 1(c) (third from top), for lower metallicity stars with [Fe/H] < -0.1, shows that the Hercules stream is predominantly seen in higher metallicity stars. The Hercules stream is also visible in the solar metallicity stars in Fig. 1(b) (the second from top) corresponding to stars with $-0.1 <$ [Fe/H] < 0.2, confirming Raboud et al. (1998), Liu (2016), Ramya et al. (2016), and Perez-Villegas et al. (2017) who find the Hercules streams consists of intermediate-to-high metallicity stars. The stream is hardest to detect in the low-metallicity stars with [Fe/H] < -0.1 shown in Fig. 1(c) (third from top).

To illustrate how the visibility of the Hercules stream depends on metallicity, we show vertical slices near longitude $\ell = 270°$ through histograms like those shown in Fig. 1. In Fig. 2, we plot one-dimensional histograms showing the tangential velocity distributions for stars in the four different metallicity ranges: [Fe/H] > 0.2, $-0.1 <$ [Fe/H] < 0.2, [Fe/H] < -0.1,and [α/Fe] > 0.2. Stars are restricted in galactic longitude to $250° < \ell < 290°$, in radial velocity to $-40 < -v_r < 10\,\mathrm{km\,s^{-1}}$, in distance to less than 1 kpc and Galactic latitude $|b| < 45°$. The histograms have been normalized so that they integrate to 1 and the bins are $3\,\mathrm{km\,s^{-1}}$ wide. In each histogram, the number of stars is 2700, 8982, 11339, and 4114 for the metal-rich, near-solar, metal-poor, and high-α metallicity stars.

The Hercules stream is the red peak in Fig. 2 at a tangential velocity $v = -v_\theta - 230 \approx -35\,\mathrm{km\,s^{-1}}$ and it is clear because of the dip at $v \approx -25\,\mathrm{km\,s^{-1}}$ separating it from stars in more nearly circular orbits at $v \sim 0\,\mathrm{km\,s^{-1}}$. A dip and peak are visible in metal-rich and near-solar metallicity stars. As there are more metal-poor stars in these histograms than metal-rich stars, the absence of a dip in the histogram at $v \sim -25\,\mathrm{km\,s^{-1}}$ in the metal-poor sample is significant. We disagree with the previous studies by Bensby et al. (2007a) and Bovy & Hogg (2010), who find no significant metallicity preference in the Hercules stream for stars in the solar neighbourhood.

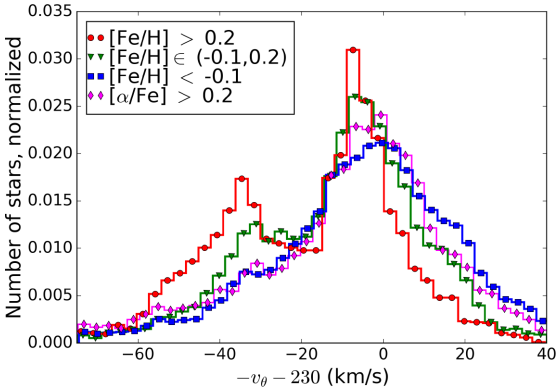

Figure 2. The distribution of tangential velocities for stars restricted in galactic longitude to $250° < \ell < 290°$, in radial velocity to $-40 < -v_r < 10\,\mathrm{km\,s^{-1}}$ and in distance to less than 1 kpc. The Hercules stream is the peak at a tangential velocity $v = -v_\theta - 230 \approx 35\mathrm{km\,s^{-1}}$ that is prominent in the supersolar metallicity stars shown in red and with round points. There are more subsolar metallicity stars (shown in blue with square points) at positive tangential velocities, corresponding to stars coming into the solar neighbourhood from the outer Galaxy. Near solar metallicity stars are shown in green with triangles and α-element-enhancedstars are shown in magenta with diamonds.

There are similar numbers of α-element-enhancedstars as supersolar metallicity stars in the histograms of Fig. 2, but many of the α-element-enhancedstars appear to have nearly circular orbits, suggesting that there might be contamination from low temperature dwarfs that have less well-measured abundance ratios. The smaller number of stars in the histograms of the α-element-enhancedstars with negative v velocities makes each velocity bin in that region more poorly sampled. Fig. 1(d) (bottom panel), illustrating velocity distributions for the high-α-element stars at different longitudes, shows that these also contain an extension to low v that is most strongly seen at galactic longitudes $240° < \ell < 280°$. This extension reaches somewhat lower tangential velocities than the Hercules stream seen in high-metallicity stars (those with [Fe/H] > 0.2 and shown in the top panel of Fig. 1a). We do not see a gap in Fig. 1(d) or a dip in Fig. 2 in the high-α-element stars. A dip must be present in the velocity distribution for us to identify a peak with the Hercules stream. We would require better measurements and sampling of the α-rich population to determine whether the Hercules stream really is absent from that stellar population.

The lack of low-metallicity stars in the Hercules stream imply that the Hercules stream is predominantly a metal-rich and thin-disc dynamical structure. We support the similar conclusion by Ramya et al. (2016); for a plot of [α/Fe] versus [Fe/H] for giant stars chosen specifically in the Hercules stream, see their fig. 7. Because of the Galaxy's metallicity gradient, higher metallicity thin disc stars are preferentially found closer to the Galactic Centre, at smaller galactic radius. Stars in the Hercules stream with negative v have lower angular momentum than a circular orbit at the solar radius. Using a circular velocity of $230\,\mathrm{km\,s^{-1}}$ a star with $v = -40\,\mathrm{km\,s^{-1}}$ and currently at radius $r = \mathrm{R}_\odot$ would have a mean orbital or guiding radius of $r_g = (230 - 40)/230 \times 8 = 6.6$ or 1.4 kpc closer to the Galactic Centre than the Sun. Using a metallicity gradient of -0.07 dex per kpc in [Fe/H] (Anders et al. 2017), stars at this guiding radius would on average have a metallicity of [Fe/H] ~ 0.1, where we are

taking a solar value of [Fe/H] = 0 at $R_\odot$ (e.g. Casagrande et al. 2011). This is only 0.1 dex away from our cut-off of 0.2 used to make the histograms shown in Fig. 1(a). At a guiding radius of 6.6 kpc, there would be fewer lower metallicity stars than at the Sun's guiding radius. The lack of metal-poor disc stars at this guiding radius likely accounts for the dominance of the Hercules stream in the higher metallicity stars compared to the lower metallicity stars.

In this discussion, we have so far neglected the role of the Galactic bar, but it is necessary to account for the gap separating the Hercules stream from the lower eccentricity stars and account for the non-zero u velocity of the stream (e.g. Dehnen 1999b). The gap is attributed to a division in phase space caused by one or more resonances with the bar (Kalnajs 1991; Dehnen 2000; Fux 2001; Perez-Villegas et al. 2017). Orbits can be classified based on their proximity to a periodic orbit or equivalently an orbit that is closed in a frame rotating with a bar. For the fast bar model, the simplest orbit families are those just outside the outer Lindblad resonance and elongated parallel to the bar and those just inside the inner Lindblad resonance that are elongated perpendicular to the bar (Kalnajs 1991; Dehnen 2000; Fux 2001). The gap seen in the velocity distribution could be associated with an unstable or chaotic region separating these two orbit families. More complex models (e.g. Fux 2001; Minchev et al. 2010) find that additional orbit families are present so it is not straightforward to associate each velocity vector (or (u, v) components) with a particular orbit shape. For the slow bar model, the gap in velocity space is associated with corotation and separates orbits circulating around the Galactic Centre from those librating about an L4 or L5 Lagrange point (see fig. 3 by Perez-Villegas et al. 2017).

The high-α-element or thick-disc population has a shorter radial exponential scale length and a higher velocity dispersion than the thin or low-α-element disc (Hayden et al. 2015, 2017). A higher velocity dispersion implies there are more stars at higher eccentricities that may be affected by resonances with the bar that can push them into the solar neighbourhood. The extension to low v and negative u in the velocity distributions of the high-α-element stars would influence measurements of velocity component averages, and is relevant for interpretation of non-circular streaming motions seen in the thick disc RAVE survey stars (Antoja et al. 2015).

4.1 The gap between the Hercules stream and other stars

Using RAVE and LAMOST survey data, Perez-Villegas et al. (2017) found that the v value of the gap separating the Hercules stream from stars on circular orbits in the velocity distribution depends on distance from the Galactic Centre, with variations seen over a distance of a few hundred pc. This sensitivity of the local velocity distribution to galactic position was also seen in their numerical model. A similar shift in v as a function of galactocentric radius was seen by Antoja et al. (2014) in RAVE survey data and predicted with a fast bar model. For stars at a galactic radius of 8.6 kpc Perez-Villegas et al. (2017) saw the gap at $v \approx -50\,\mathrm{km\,s^{-1}}$, whereas at a radius of 7.8 kpc (with their adopted solar radius of 8.2 kpc), the gap was at $v \approx -30\,\mathrm{km\,s^{-1}}$. Thus, they found that the gap v velocity increased (was less negative) with decreasing galactic radius.

An orbital resonance is defined by a commensurability between orbital frequencies. Equivalently there is an integer relation between orbital and epicyclic periods and the period of a perturbation, here the Galactic bar. In the Galactic disc, the orbital period is approximately set by the angular momentum. So a division in phase space at a particular angular momentum could be associated with a resonance with the bar. The dependence of the velocity distribution on the radius of the neighbourhood suggests that the Hercules stream or the gap separating it from circular orbits is set by a particular angular momentum value. To test this hypothesis, we use the GALAH stars to make histograms of angular momentum versus a normalized energy difference $(E - E_c(L))/v_c^2$ that is approximately equal to the square of orbital eccentricity (see equation A13). The energy E is the energy per unit mass restricted to velocity components in the plane (defined in equation A1), and $E_c(L)$ (equation A12) is the energy per unit mass of a circular orbit with angular momentum L. The z-component of angular momentum per unit mass is $L = |rv_\theta|$ and computed from the a star's galactocentric radius r and tangential velocity v_θ. We compute the energy difference approximating $E_c(L)$ for a flat rotation curve with circular velocity $v_c = 230\,\mathrm{km\,s^{-1}}$. We use $V_{\mathrm{circ},\odot}$ specifically for the LSR's circular velocity and $v_c = V_{\mathrm{circ},\odot}$ for the circular velocity when we approximate the Galaxy with a flat rotation curve.

Fig. 3 shows the number of stars in different angular momentum and energy difference bins. This figure is similar to a Toomre diagram where $u^2 + w^2$ is plotted against v (see fig. 2 by Bensby et al. 2007a). Our histograms in Fig. 3 show the number of stars in bins that are $5\,\mathrm{km\,s^{-1}}$ kpc wide in angular momentum and 0.001 wide in the energy difference (approximately the orbital eccentricity squared or e^2). Stars are restricted to distances $d < 1$ kpc and latitudes $|b| < 45^\circ$ (and the GALAH survey itself contains few stars with $|b| < 10^\circ$). There is no cut in galactic longitude. The y-axes of each panel show the angular momentum in units of $\mathrm{km\,s^{-1}}$ kpc. The x-axes are unitless as the energy difference has been normalized by v_c^2. The number of stars used to make each histogram in Fig. 3 is shown in green on the lower left of each panel. Again the histograms are normalized so that they integrate to 1. Three normalized histograms are shown, the top one is for high-metallicity stars with [Fe/H] > 0.2, the middle one is for lower-metallicity stars with [Fe/H] < −0.1,and the bottom one is for high-α-element stars with [α/Fe] > 0.2. In the topmost histogram, the right axis shows the guiding radius r_g computed from the angular momentum and assuming a flat rotation curve ($r_g(L) = L/v_c$). The top axis shows the orbital eccentricity assuming that the energy difference is the square of the eccentricity.

Fig. 3 shows that both the high-metallicity and α-element-richstars show extensions to low angular momentum, corresponding to stars coming from the inner Galaxy. At low metallicity, there are more stars with higher angular momentum, corresponding to stars coming into the solar neighbourhood from the outer Galaxy. The top panel lets us estimate the angular momentum of a gap separating the Hercules stream from more circular orbits at about $L_{\mathrm{gap}} \sim 1600\,\mathrm{km\,s^{-1}}$ kpc. We now use the gap angular momentum value to estimate the location of the gap in the different local neighbourhoods that are seen at each galactic longitude in Fig. 1(a).

4.2 The Hercules stream seen in different directions

Each velocity distribution shown in Fig. 1(a) was constructed of stars from a different region in galactic longitude. The (x, y) position in galactic coordinates of the centre of each region can be estimated from the central galactic longitude l and the mean distance of the stars from the Sun, d_n;

$$x(l) = d_n \cos l - \mathrm{R}_\odot,$$
$$y(l) = d_n \sin l. \qquad (2)$$

The galactocentric radius of the neighbourhood is estimated with $r(l) = \sqrt{x(l)^2 + y(l)^2}$. The location of the gap in v is set by its

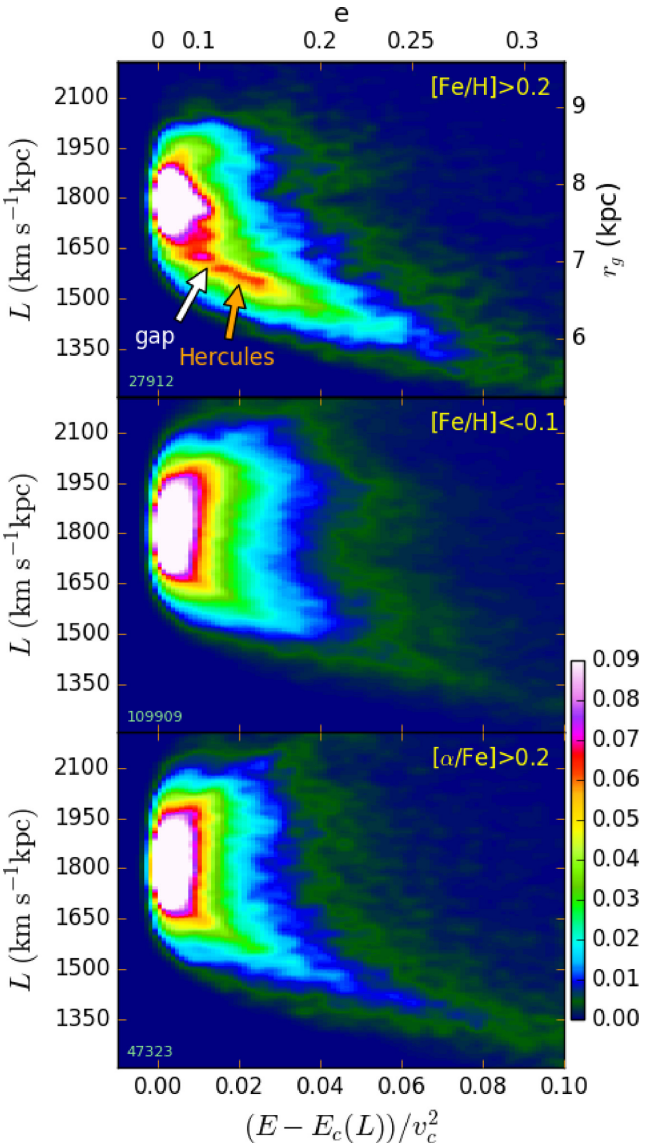

Figure 3. Histogram of stars in angular momentum and energy bins. The x-axes are the difference between orbital energy in the plane and that of a circular orbit normalized by v_c^2. The y-axes are angular momentum (the z-component) in units of km s^{-1} kpc. The top panel shows higher metallicity stars with Fe/H] > 0.2, the middle one is for lower metallicity stars with [Fe/H] < -0.1 and the bottom one is for high-α-element stars with [α/Fe] > 0.2. Green numbers in each panel on the lower left are the number of stars used to make the histogram. The high-metallicity and high-α-element stars show extensions to low angular momentum and higher energy, corresponding to higher eccentricity stars from the inner Galaxy reaching into the solar neighbourhood. There are more high angular momentum, low-metallicity stars corresponding to stars from the outer Galaxy coming into the solar neighbourhood. There is a gap at about 1600 km s^{-1}kpc separating the Hercules stream from the more circular orbits. In the topmost histogram, the right axis shows guiding radius computed from the angular momentum and assuming a flat rotation curve. The top axis shows orbital eccentricity, computed with energy difference equal to the square of the eccentricity and for a flat rotation curve.

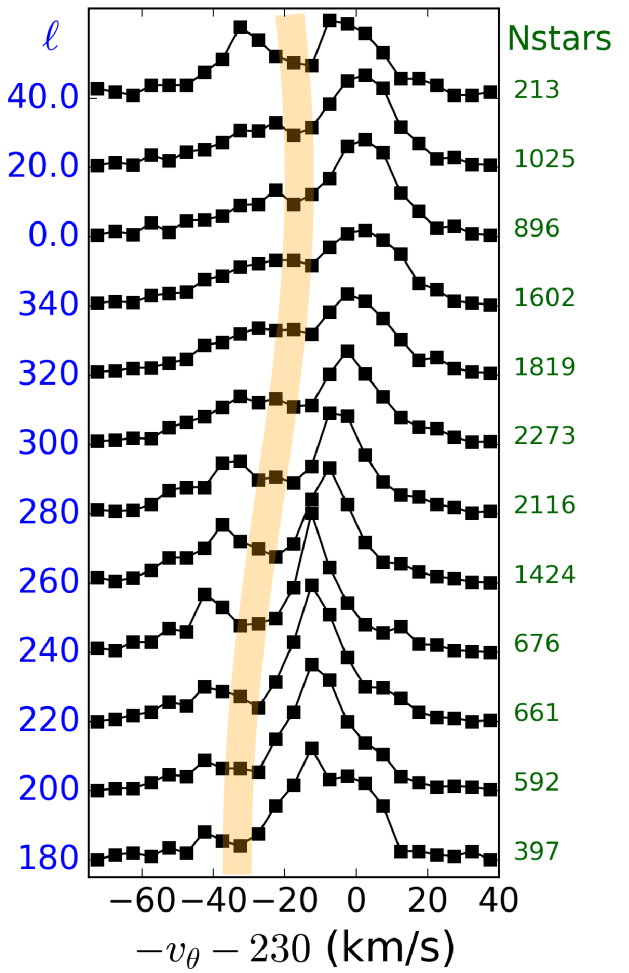

Figure 4. The uv velocity distributions of stars with distances $d < 500$ pc and [Fe/H] > 0.2 as a function of galactic longitude. The orange line (computed with equation 3) corresponds to a gap angular momentum value of $L_{\rm gap} = 1640$ km s^{-1} kpc. The line curves because the galactocentric radius of each neighbourhood depends on the viewed longitude. The line suggests that the gap between the Hercules stream and circular orbits is set by a particular angular momentum value, as would be expected with a bar resonant model.

angular momentum with gap velocity as a function of galactic longitude

$$v_{\rm gap}(l) = \frac{L_{\rm gap}}{r(l)} - v_c, \tag{3}$$

where we use a circular velocity of $v_c = 230$ km s^{-1}. Fig. 4 shows the curve $v_{\rm gap}(l)$ plotted on top of the (u, v) histograms we showed previously in Fig. 1(a) for the high-metallicity stars with distances $d < 500$ pc. The curve was computed using a distance of $d_n = 340$ pc which is the median distance from the Sun of stars used to make the histograms. In Fig. 5, we show normalized tangential velocity distributions (similar to that shown in Fig. 2) but constructed for stars at different galactic longitudes. Each distribution is restricted to stars with [Fe/H] > 0.2, $d < 500$ pc, $-40 < u < 10$ km s^{-1}, and galactic longitude within 20° of the value given in blue on the left axis. The numbers of stars in each histogram are given in green on the right axis. The orange line shows the gap v value computed using equation (3).

Figs 4 and 5 show that the gap separating the Hercules stream from circular orbits is reasonably well approximated using the

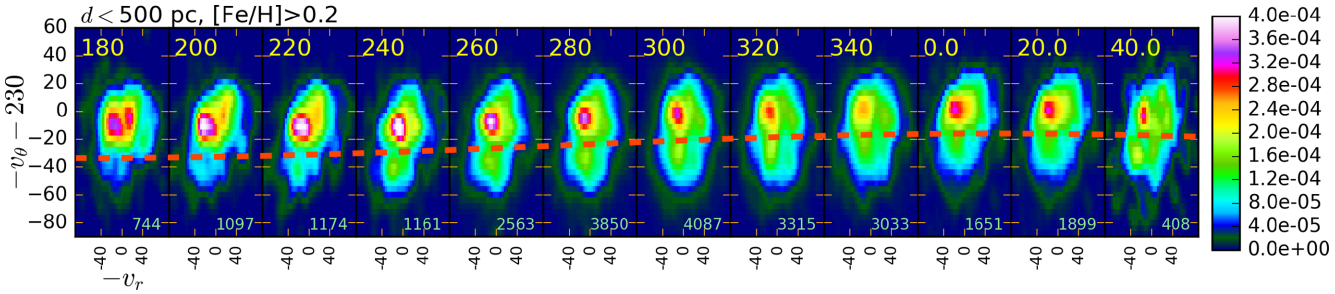

Figure 5. Normalized tangential velocity distributions are shown for stars at each galactic longitude given in blue on the left axis. The numbers of stars in each histogram is shown on the right axis. The vertical range is not shown on either axis. These distributions are similar to that shown in Fig. 2 except they are for stars at different galactic longitudes. The thick orange line is computed with equation (3) and corresponds to a gap angular momentum value of $L_{\rm gap} = 1640\,{\rm km\,s^{-1}}$ kpc. The Hercules stream forms the peaks at around $v \sim -40\,{\rm km\,s^{-1}}$ that are prominent near galactic longitude $\ell = 270^\circ$.

angular momentum value of $L_{\rm gap} = 1640 \pm 40\,{\rm km\,s^{-1}}$ kpc where we have estimated the error by eye after plotting curves for higher and lower angular momentum values.

Is the angular momentum value of the gap $L_{\rm gap} = 1640 \pm 40\,{\rm km\,s^{-1}}$ kpc consistent with fast and slow bar models for the Hercules stream? For the fast bar, the Hercules stream is caused by the outer Lindblad resonance (Kalnajs 1991; Dehnen 1999b, 2000) which is important for stars with angular rotation rate near Ω that satisfies a resonant condition

$$2(\Omega - \Omega_{\rm b}) + \kappa \sim 0. \quad (4)$$

For a flat rotation curve with $\kappa/\Omega = \sqrt{2}$ the resonant condition is equivalent to

$$\Omega_{\rm b}/\Omega = 1 + \frac{1}{\sqrt{2}} \approx 1.71. \quad (5)$$

Multiplying by $v_{\rm c}^2$ and setting $L_{\rm gap} = v_{\rm c}^2/\Omega$ for the resonant orbits with angular rotation rate Ω, we can manipulate this expression to estimate

$$L_{\rm gap} \approx \left(1 + \frac{1}{\sqrt{2}}\right) \frac{v_c^2}{\Omega_{\rm b}}. \quad (6)$$

Using a fast bar pattern speed $\Omega_{\rm b} = 56\,{\rm km\,s^{-1}\,kpc^{-1}}$ (Antoja et al. 2014) and circular velocity $v_{\rm c} = 230\,{\rm km\,s^{-1}}$, equation (6) gives a gap angular momentum of $1613\,{\rm km\,s^{-1}}$kpc, which is consistent with our estimate for the gap angular momentum value (1640; estimated in Fig. 3 and shown as a line in Figs 4 and 5). Our estimated gap angular momentum is consistent with previous estimates of $\Omega_{\rm b}$ for a fast bar pattern speed and an outer Lindblad resonance model for the Hercules stream.

For the slow bar, with an estimated bar pattern speed of $\Omega_{\rm b} = 39\,{\rm km\,s^{-1}\,kpc^{-1}}$ (Perez-Villegas et al. 2017), the Hercules stream is associated with stars at corotation and librating about a Lagrange point. The angular momentum associated with corotating orbits

$$L_{\rm CR} = \frac{v_{\rm c}^2}{\Omega_{\rm b}} = 1356\ {\rm km\ s^{-1}\ kpc}, \quad (7)$$

which is lower than our estimated gap angular momentum of $1640\,{\rm km\,s^{-1}}$ kpc. The Hercules stream stars themselves have somewhat lower angular momentum values of about $1550\,{\rm km\,s^{-1}}$ kpc than our estimated gap value, and both of these exceed the angular momentum associated with corotation in the slow bar model. Our estimated gap angular momentum does not support a corotation model for the Hercules stream. Perhaps more careful orbital modelling is needed to account for the velocity distribution as the orbits in the corotation region have high amplitudes of libration about the Lagrange points (see Perez-Villegas et al. 2017; Portail et al. 2017a,b).

The Hercules stream was detected using APOGEE giant stars that are a few kpc away and seen along a galactic longitude of 270° (Hunt et al. 2018). Stars that are 3 kpc in the 270 degree direction would have a galactocentric radius of 8.5 kpc, outside that of the Sun. At this radius, equation (3) gives a v value of $-40\,{\rm km\,s^{-1}}$ for the gap velocity, somewhat larger than the gap $v \approx -27\,{\rm km\,s^{-1}}$ at $\ell = 270^\circ$ estimated for the nearer GALAH stars. We made a similar set of histograms for high-metallicity GALAH stars with distance between 1 and 3 kpc. In those the Hercules stream is less noticeable and the gap separating it from the stars on circular orbits not visible in the histograms. However, there are only 1500 stars in the histogram at $\ell = 260^\circ$ as the magnitude limited GALAH survey contains fewer giants than main sequence stars, so the lack of structure is not significant. Stars 3 kpc away from the Sun in the 270° direction are located at a galactic azimuthal angle θ of 20° (measured from the Sun galactic centre line) and the azimuthal angle in the Galaxy too should affect the velocity distribution. We do not confirm, but neither do we dispute the detection of the Hercules stream in giant stars a few kpc from the Sun by Hunt et al. (2018).

5 STRUCTURE IN VELOCITY DISTRIBUTIONS OF NEARER STARS (D < 250 PC)

The velocity distributions in Fig. 1 do not obviously exhibit the clumps identified in the *Hipparcos* satellite observations of nearby and brighter stars that corresponded to moving groups or stellar kinematic associations previously identified by Olin Eggen (Eggen 1958a,b,c, 1965a,b,c, 1995, 1996) (see fig. 3 and table 2 by Dehnen 1998 and fig. 7 and table 1 by Famaey et al. 2005). To investigate this issue we look at velocity distributions for a nearer GALAH sample of stars. Fig. 6 shows three sets of velocity distributions similar to those in Fig. 1 but for distances $d < 250$ pc instead of 500 pc. Fig. 6(a) (top row) shows metal-rich stars with [Fe/H] > 0.2, Fig. 6(b) (middle row) shows near solar metallicity stars with $-0.1 <$ [Fe/H] < 0.2, and Fig. 6(c) (bottom row) shows lower metallicity stars with [Fe/H] < -0.1. These histograms are constructed with $3\,{\rm km\,s^{-1}}$ square bins in (u, v) velocity components. We did not make a similar figure for high-α-element stars due to the lower numbers of stars in the histograms (which were noisy).

Clumps in velocity distributions are often designated by the name of a star or cluster that has similar space motions or by a direction

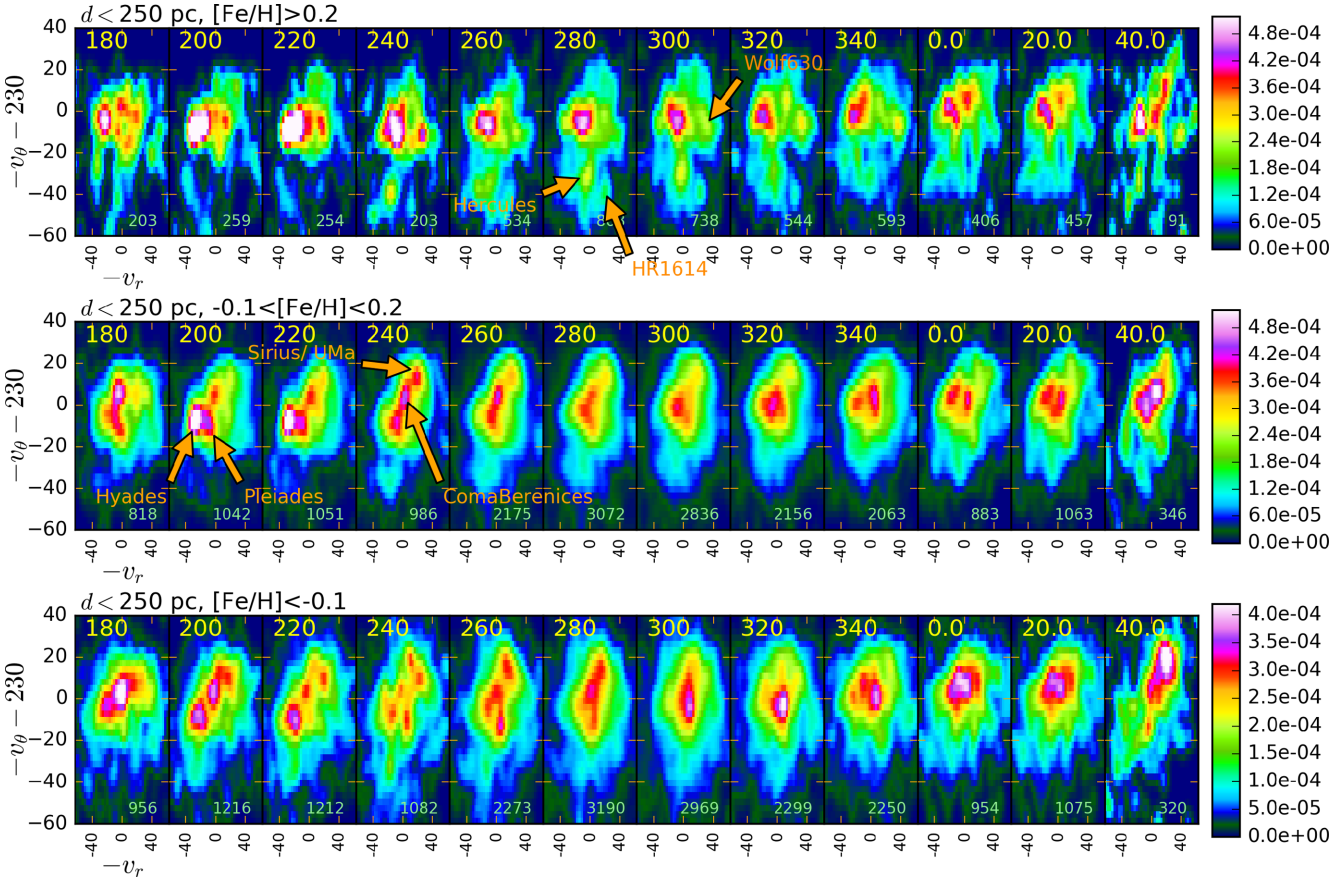

Figure 6. Velocity distributions in uv similar to those in Fig. 1 but for nearer stars with distances $d < 250$ pc. (a) For metal-rich stars with [Fe/H] > 0.2. (b) For near solar metallicity stars $-0.1 <$ [Fe/H] < 0.2. (c) For metal-poor stars with [Fe/H] < -0.1.

on the sky where members have been discovered (Eggen 1965c). These clumps are called moving groups, streams, stellar associations, or superclusters (Eggen 1965c; Dehnen 1998; Famaey et al. 2005). In the velocity distributions shown in Fig. 6, the moving groups called Hyades, Pleiades, Coma Berenices, and Sirius/UMa by Dehnen (1998) are visible and are labelled in the near solar metallicity row of Fig. 6(b). We have labelled the Hercules stream in the metallicity-rich histograms of Fig. 6(a). There is an extension to the Hercules stream at $(u, v) \sim (20, -50)$ km s^{-1} which we tentatively identify with the HR1614 moving group, and this too is labelled on Fig. 6(a). Famaey et al. (2005) labelled the Pleaides and Hyades moving groups discussed by Dehnen (1998) as a single association called the Hyades–Pleiades supercluster, the Coma Berenices group discussed by Dehnen (1998) approximately corresponds to their Y group, and the Sirius/UMa group to their Sirius supercluster (as listed in their tables 1 and 2 and shown in their fig. 9). The Hyades, Pleiades, Sirius, Hercules, and HR1614 groups were also identified in LAMOST survey data by Liang et al. (2017). The v velocity components of our groups are lower by about 20 km s^{-1} from those reported by Dehnen (1998), Famaey et al. (2005), Liang et al. (2017) as our adopted value for the peculiar motion of the Sun and the galactic circular velocity at $R_\odot$ differs from theirs (Dehnen 1998 used $V_{\mathrm{circ},\odot} = 200$ km s^{-1} and $v_{\odot,\mathrm{pec}} = 5.2$ km s^{-1} both somewhat lower than our adopted values of $V_{\mathrm{circ},\odot} = 230$ and $v_{\odot,\mathrm{pec}} = 10$ km s^{-1}).

Fig. 6(a) shows an additional peak in the velocity distribution of high metallicity stars near $(u, v) = (26, -7)$ km s^{-1} and for $220^\circ < \ell < 340^\circ$. We tentatively identify it as Wolf 630 as its location is approximately consistent with the group of the same name identified by Liang et al. (2017). The group is denoted Group 6 by Dehnen (1998). The space motion measured by Bubar & King (2010) for the Wolf 630 moving group [their $(u, v) \sim (25, -36)$ km s^{-1}] is equivalent to our $(u, v) \sim (25, -16)$ km s^{-1} with our velocity convention. This is sufficiently near our peak's (26,−7) km s^{-1} to be consistent. We primarily see the Wolf 630 group in the nearby higher metallicity stars, though Bubar & King (2010) found a fairly broad metallicity distribution centred at near solar values (see their fig. 4).

In the nearby GALAH stars, we recover the moving groups and streams previously seen in *Hipparcos* observations. However, stars observed by *Hipparcos* are brighter than a V mag of 7 and are much brighter than the GALAH survey stars. There should be little overlap in the two samples. The GALAH detection of the these streams and groups confirms the existence of these structures in the solar neighbourhood's velocity distribution.

Fig. 6 shows that the moving groups or stellar associations identified by Olin Eggen and seen in the *Hipparcos* stars are primarily seen in near solar or lower metallicities and at galactic longitudes $200^\circ < \ell < 260^\circ$, though the Hyades group also contains higher metallicity stars. The Hercules stream and the HR1614 moving group at negative v are also seen, but primarily in the high-metallicity stars and near galactic longitude $\ell \sim 270^\circ$. The Wolf 630 moving group group, near $v \sim 0$, is also most visible in the high- metallicity stars but at $240^\circ < \ell < 340^\circ$.

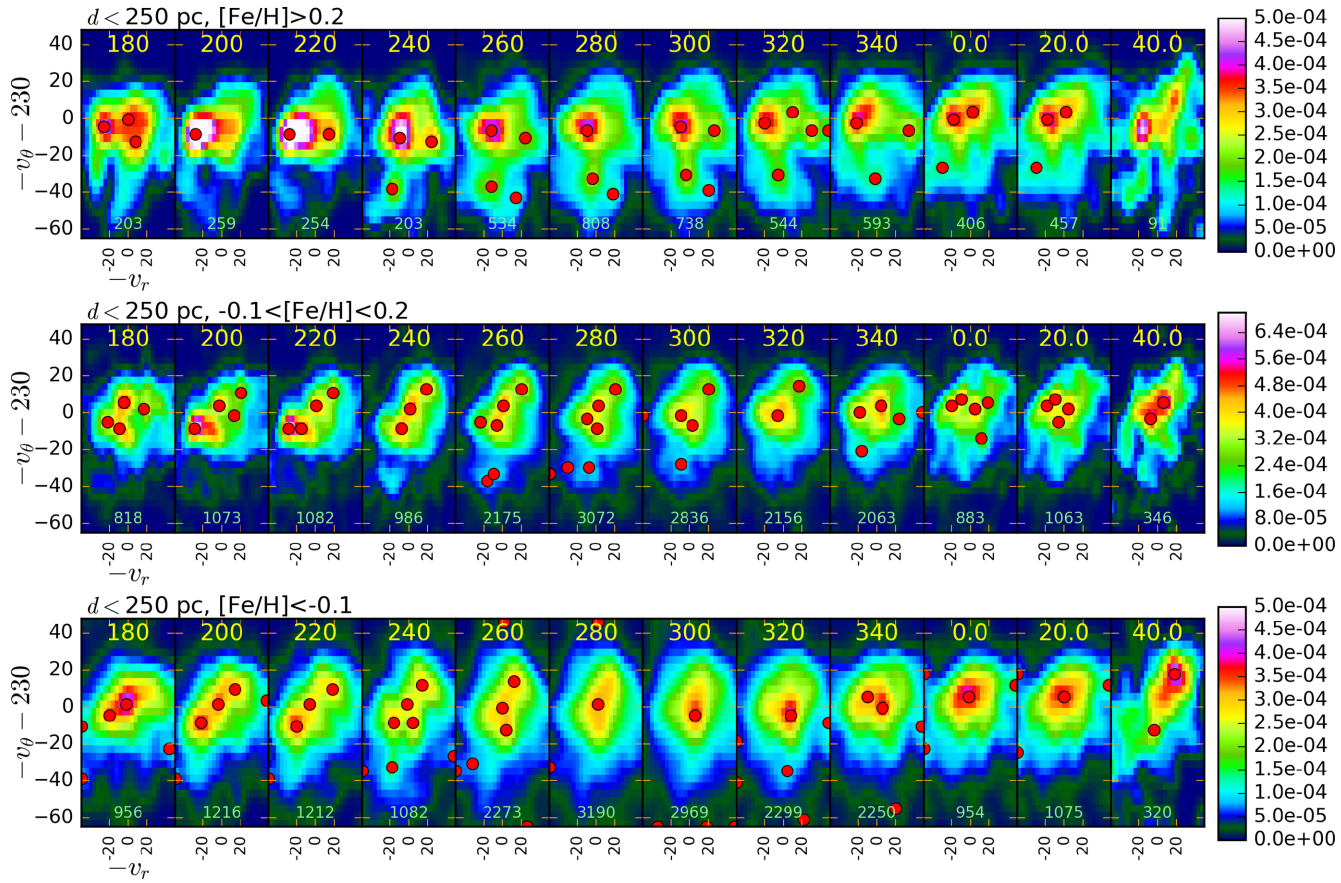

Figure 7. Peaks are found in the *uv* velocity distributions of nearby stars that are shown in Fig. 6. Red dots show the (u, v) velocities of the peaks and they are plotted on top of the velocity distributions.

The Hercules stream is the only stream that is prominent in the more distant sample (comparing Fig. 1(a) for $d < 500$ pc to Fig. 6(a) for $d < 250$ pc). The stream is evident in local velocity distributions for galactic longitudes $\ell < 240^\circ$ and $\ell > 340^\circ$ but not identified as a peak outside this range. There is some ambiguity on the u value of the Hercules stream. Dehnen (1998) and Famaey et al. (2005) identify two groups at $v \sim -50\,\mathrm{km\,s^{-1}}$. One is at $u \sim -40\,\mathrm{km\,s^{-1}}$ and denoted Group 8 by Dehnen (1998), denoted Group He by Famaey et al. (2005), and consistent that denoted Hercules I by Liang et al. (2017). The other group is at $u \sim -20\,\mathrm{km\,s^{-1}}$ and is denoted Group 9 by Dehnen (1998), group HV by Famaey et al. (2005), and Hercules II by Liang et al. (2017). The studies by Dehnen (1998) and Famaey et al. (2005) were both using *Hipparcos* observations, so we could expect similar clump identifications. Using LAMOST survey data, Liang et al. (2017) identified two additional and weaker clumps associated with the Hercules stream.

The Hyades stream has the same velocities as the open cluster M67, though we have been careful to remove a K2-HERMES field that serendipitously contained M67 stars in the near solar metallicity histograms (see Table C1 for the list of figures affected by this cut). The GALAH survey contains few stars that are identified members of open or globular clusters (Kos et al. 2018). The paucity of serendipitously observed cluster stars in the GALAH sample is due to logistics associated with fibre positioning and scheduling. So we are confident that the peaks seen in the nearby stars are not due to contamination by bound cluster members. This contrasts with the *Hipparcos* survey that specifically targeted young clusters, including the Pleiades and Hyades clusters (Perryman et al. 1997).

In our velocity histograms or distributions, we identify the Hyades, Pleaides, Coma Berenices, Sirius/UMa, Wolf 630, and HR1614 streams or moving groups in the very nearby stars ($d < 250$) and these groups were much more difficult to see in the more distant $d < 500$ pc sample. As the GALAH survey (neglecting targeted clusters) has few cluster members, we can regard these moving groups as fine structure in the local velocity distribution that is both metallicity dependent and dependent on position in the Galaxy, varying over distances of a few hundred pc. We infer that this structure varies on short distances because the appearance of the velocity distributions varies as a function of galactic longitude.

In the more distant samples (Fig. 1), the velocity distributions appear smoother and with less fine structure than in Fig. 6. Errors in distances and tangential velocities, which are larger for the more distant samples, could smooth out substructure in the velocity distribution. Our more distant sample covers a wider volume causing coarse graining or averaging in the velocity distribution, and this too would blur substructure. More distant stars tend to be located at higher elevations from the Galactic plane. The galactic longitude range of our stars $10^\circ < |b| < 45^\circ$ corresponds to vertical distances $87 \lesssim |z| \lesssim 350$ pc for stars at a distance $d = 500$ pc and $43 \lesssim |z| \lesssim 180$ pc for stars at $d = 250$ pc. At the larger distances of Fig. 1, the high galactic latitude directions should contain few thin-disc stars. Stars more distant from the Galactic plane may be less sensitive to perturbations associated with spiral structure, so veloc-

ity distributions at high $|z|$ may be smoother than those at low $|z|$. Future *Gaia* observations will allow us to confirm our findings and search for similar fine substructure in more distant neighbourhoods.

5.1 Peaks in the velocity distributions

To investigate how a clump in the local velocity distributions varies with location in the Galaxy, we identify the velocities of peaks in the histograms. We smooth the histograms in Fig. 6 by a few km s^{-1}. We flag a peak in the velocity distribution if all adjacent bins are lower than that in the bin and if the number of counts in the bin is higher than a threshold value that we adjusted separately for each metallicity sample. The results of this unsophisticated peak finding routine are shown in Fig. 7, where we plot as red dots the position of peaks on top of the velocity distributions. The peaks are listed in Tables D1–D3 in Appendix D.

The peaks shown in Fig. 7 illustrate that the moving groups that are prominent in the velocity distributions are dependent on both viewing direction and metallicity. The Sirius/UMa group is primarily seen in solar or low-metallicity stars, confirming previous metallicity studies (King & Schuler 2005; Tabernero et al. 2017), and is seen at galactic longitudes $200^\circ < \ell < 300^\circ$. The Coma Berenices group is primarily seen in low-metallicity stars in a similar galactic longitude range. The Hyades group or supercluster is seen at all metallicities, confirming previous studies (De Silva et al. 2011; Pompeia et al. 2011; Tabernero, Montes & González Hernández 2012). The Hercules stream is most prominent at higher metallicity and near $\ell \sim 270^\circ$. The stream is seen at most galactic longitudes in the velocity distributions, but in many directions, it is a plateau in the velocity distribution rather than a peak.

The peak finding routine finds an additional peak near the Hercules stream but at lower v and at positive u. This clump could be the HR1614 moving group (Eggen 1998; De Silva et al. 2007), though the clump we see is near $u \sim +20$ km s^{-1} whereas previous studies find that the group is a narrow but tilted feature in the uv plane that ranges from $u \sim -50$ to $u \sim 20$ km s^{-1} with v increasing from -70 to -50 km s^{-1} (see fig. 5 by De Silva et al. 2007). This clump in our velocity distribution appears compact, suggesting that its progenitor is an old and recently disrupted open cluster. If so its survival prior to disruption is a puzzle. Its age is estimated at 2 Gyr (De Silva et al. 2007) but even a massive star cluster born in the disc is unlikely to survive that long (Fujii & Portugies Zwart 2016). Streams or clumps in the velocity distribution are also seen in the low-v, high-α stars at a similar u value as the HR1614 clump. If the high-α stars (see Fig. 1d) contain similar structure to the high-metallicity stars, then a bar-induced mechanism for the HR1614 clump would be more likely than a chemically homogeneous recently disrupted cluster. As the GALAH survey continues, improved abundance measurements (probing for chemical homogeneity) and observation of additional high-α stars improving the appearance of the velocity distribution would allow us to tell these two possibilities apart.

Each peak identified in the histograms in Fig. 6 has specific u, v values and these are a velocity vector or a direction of motion. To visualize the directions of motion, we plot the peaks as vectors in Fig. 8. The x- and y-axis coordinates are centred about the Sun with positive x towards the Galactic Centre and positive y in the direction of rotation. The colour of the vectors is set by the metallicity with red corresponding to peaks seen in higher metallicity stars, green for near solar metallicity stars, and blue for lower metallicity stars. Coloured arrows in Fig. 8 are shown for most of the identified peaks in Fig. 7 (we excluded a few high velocity ones that were at positions with low numbers of stars in the histograms). Coloured arrows pointing to the right correspond to motions towards the Galactic Centre (with positive u or negative v_r) and arrows pointing upwards correspond to motion faster than Galactic rotation (positive v).

In Fig. 8, neighbourhoods in the Galaxy are shown as grey filled circles at a distance of 200 pc from the Sun (just within the 250 pc limit for the histograms of Fig. 6). We show a grey circle for each central galactic longitude (for which we made histograms) and these range from $l = 180^\circ$ on the left to $l = 40^\circ$ on the upper right. The grey circles represent the neighbourhoods and the coloured arrows represent the space motions of stars in these neighbourhoods. The velocities of the moving groups are shown as directions in an illustration in the right-hand panel of Fig. 8.

Fig. 8 shows smooth variations in the directions and lengths of space motions that are peaks in the local velocity distributions. For example, Hyades and Sirius/UMa moving groups in the low-metallicity stars (blue arrows) are primarily seen on the left (at galactic longitudes $180 < \ell < 280^\circ$),but the direction of each arrow smoothly varies between $\ell = 180^\circ$and 280°. The Sirius/UMa group velocity increases in v and decreases in u with increasing longitude ℓ. The Hercules stream and HR1614 moving group peaks increases in both u and in v with increasing galactic longitude. The Hyades supercluster, seen at all metallicities, increases in v with increasing galactic longitude ℓ. This figure illustrates in a different way that structure in velocity distributions varies as a function of location in the Galactic disc.

In Fig. 9, u and v velocity components for the same peaks seen in velocity distributions of Figs 6 and 7 are plotted against galactic longitude l. Small triangles show peaks in the low-metallicity stars, squares show the near solar metallicity stars, and large circles show the higher metallicity stars. In the left-hand panel, showing u versus l, points are coloured by their v value and the colour scale shown with the accompanying colourbar. In the right panel, showing v versus l, points are coloured by their u value. The moving groups and streams are easiest to identify in the right hand panel showing v versus galactic longitude. Over the range in galactic longitude where a peak is seen, peak v velocities tend to increase with increasing galactic longitude. Trailing spiral arms might exhibit such a trend, though a similar trend is seen in the Hercules stream and that one is associated with the Galactic bar. The point colours make some streams stand out. The Wolf 630 group can be seen on the right-hand panel as red circles in the same region as the Hyades and Pleiades groups. The Hercules stream and the HR1614 group can be seen in the left-hand panel as blue circles near $l = 270^\circ$.

The HR1614 group peaks (the three lowest red points in the right-hand panel of Fig. 9) have u increasing with v. Fitting a line to these three points in the form $v = a + bu$ (as did De Silva et al. 2007 for HR1614 candidate stars in their fig. 5),we estimate a slope of $b \approx 2/3$, exceeding the slope of $b = 0.18$ measured by De Silva et al. (2007). De Silva et al. (2007) measured the slope (in velocity space) of a local distribution of bright and nearby stars, whereas we have measured a slope in the way peak velocity components vary with galactic longitude for stars a few hundred pc away from the Sun. The two measurements are not equivalent. The slope measured by De Silva et al. (2007) was probably not due to stellar velocities varying systematically with distance from the Sun.

The local neighbourhoods at $l = 180^\circ$ and 0° are separated by about 400 pc. The variations in u, v values for the different stream peaks have differences of size $\Delta \sim 10$ km s^{-1}. Dividing the velocity change by the distance between neighbourhoods gives us gradient in velocity. The gradient in the velocity components for the stream peaks has a size scale of order $\frac{\mathrm{d}v}{\mathrm{d}x} \sim 25$ km s^{-1} kpc^{-1}.

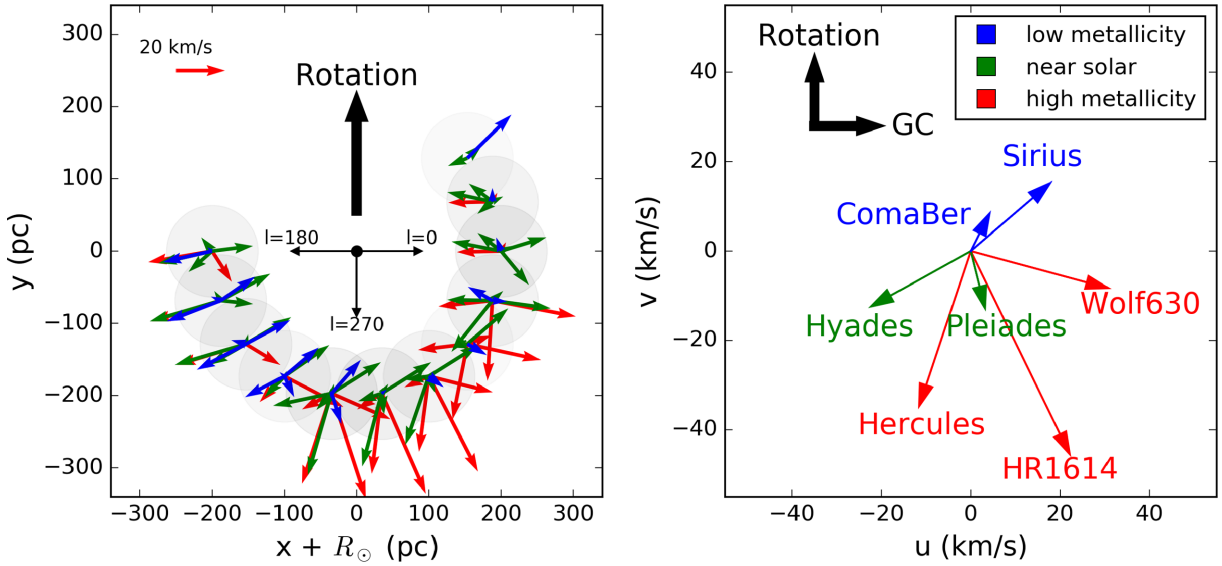

Figure 8. (a) Left-hand panel: Peaks seen in the $d < 250$ pc uv velocity distributions of Figs 6 and 7 are drawn as a function of position in the Galaxy. The x- and y- axis coordinates are centred about the Sun with positive x towards the Galactic Centre and positive y in the direction of rotation. Green arrows show the velocity vectors for peaks in the velocity distribution for solar metallicity stars. Blue arrows are for peaks in the lower metallicity set ([Fe/H] < -0.1) and red arrows are for peaks in the higher metallicity set ([Fe/H] > 0.2). Coloured arrows are shown for the peaks we identified in Fig. 7. Arrow length depends on the u, v velocity vector length. The red arrow on the upper left shows a velocity vector of length 20 km s^{-1}. Coloured arrows pointing to the right correspond to motions towards the Galactic Centre and arrows pointing upwards correspond to motion faster than Galactic rotation. Neighbourhoods are shown as grey filled circles at a distance of 200 pc from the Sun and at galactic longitudes ranging from $\ell = 180°$ (on the left) to 40° on the upper right. Each grey circle represents the location of stars that we see in a particular direction. The smaller black arrows in the centre show the directions of the different galactic longitudes. (b) Right-hand panel: The illustration shows the directions of velocity peaks and we have labelled them with the names of moving groups or streams. In this panel, thick black arrows show the direction of rotation and the direction of the Galactic Centre.

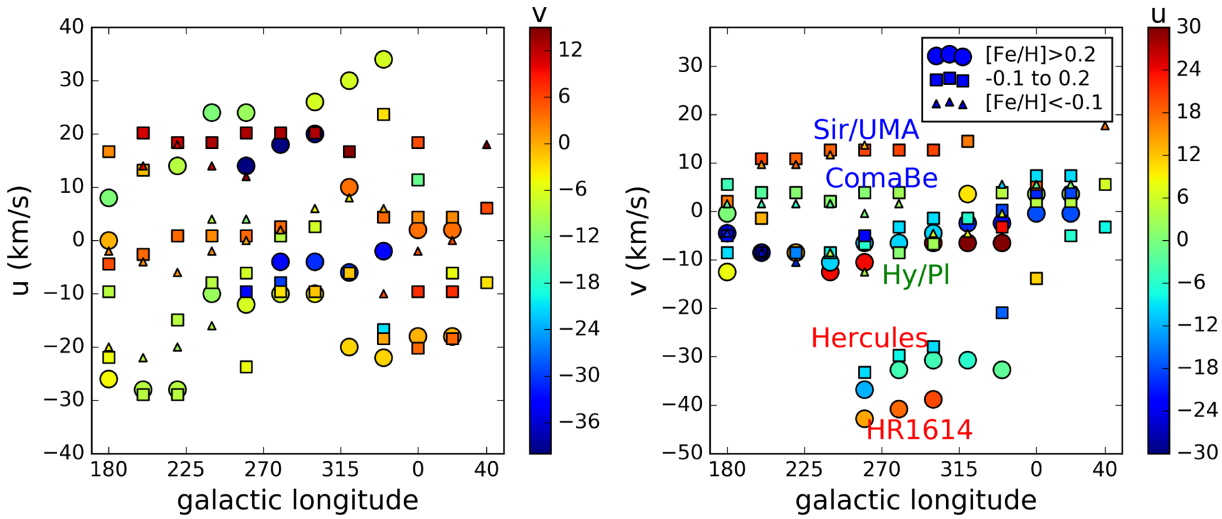

Figure 9. Peaks seen in the $d > 250$ pc uv velocity distributions of Figs 6 and 7 have $u = -v_r$ velocity component plotted as a function of galactic longitude in the left-hand panel. The colour of the points depends on the v velocity (with $v = -v_\theta - 230$ km s^{-1} as before) and with numbers on the colourbar in km s^{-1}. In the right-hand panel, the peak v velocity is plotted as a function of galactic longitude and with colour set by the u velocity. In both panels, small triangles are for peaks in the lower metallicity set of histograms ([Fe/H] < -0.1), squares are for near solar metallicities ($-0.1 <$ [Fe/H] < 0.2) and large circles are for peaks in the higher metallicity set ([Fe/H] > 0.2). Sirius/UMa, Coma Berenices, Hyades/Pleiades, Hercules, and HR1614 streams or moving groups are most easily identified in the right-hand panel, where they are labelled. The peak v velocities of each group varies as a function of galactic longitude, with v increasing with increasing longitude over the range (in galactic longitude) where the group is distinctly seen in the local velocity distribution. The Wolf 630 group can be seen on the right-hand panel as red circles in the same region as Hyades and Pleiades. The Hercules stream (with negative u) and the HR1614 group (with positive u) can be seen in the left-hand panel as blue circles near galactic longitude $\ell = 270°$.

A worry is that a possible bias in the distance estimates could induce direction-dependent trends in the velocity components that we have misinterpreted in terms of spatial gradients in the velocity distribution. If distances are overestimate, then u would be higher at $l = 270°$ than the correct value and u would be correct at $l = 0°, 180°$ as it depends only on the radial velocity and not on the

proper motion. The v component would be high at $l = 0°$, 180°, and correct at $l = 270°$. The trends for the peaks we show in Fig. 9 are inconsistent with over- or underestimated distances. If a star has $v_{\rm tan} = 30\,{\rm km\,s^{-1}}$, an error in the distance of 30 per cent would be required to cause a $10\,{\rm km\,s^{-1}}$ error in the star's velocity u velocity component. Thus, extreme distance biases would be required to influence the velocities sufficiently to mimic the trends we see in Fig. 9.

The Sun lies just inside the Local Spiral Arm (hereafter the Local Arm), is about 2 kpc away from and inside the Perseus arm, and is outside (again about about 2 kpc away) from the Sagittarius arm (see e.g. fig. 2 by Xu et al. 2016). The Local Arm, containing the Orion stellar association and sometimes called the Orion spur, is the nearest spiral arm to the Sun (Oort, Kerr & Westerhout 1958; Russeil 2003; Vazquez et al. 2008; Xu et al. 2013; Hou & Han 2014; Xu et al. 2016). This arm is usually discussed as a spur or arm segment that may arch between the Perseus and Carina spiral arms (Vazquez et al. 2008; Hou & Han 2014); however, parallax measurements of young stars with bright molecular maser emission suggest that the Local Arm may be separate and stronger than previously inferred (Xu et al. 2013, 2016). The Sun is interior to the Local Arm by about 500 pc with nearest associated stars seen in the Galactic anticentre direction. The Sun is nearest the trailing sides of the Local and Perseus arms, but nearest the leading side of the Sagittarius arm.

N-body simulations containing spiral arms exhibit radial velocities that generally point outwards on the trailing side of spiral arms (and vice versa for the leading side) and rotational or tangential velocities which are slower than the mean on the trailing side of spiral arms (and vice versa for the leading side; Grand, Kawata & Cropper 2014; Grand et al. 2015). This gives $u < 0$, $v < 0$ in a neighbourhood on the trailing side and $u > 0$, $v > 0$ on the leading side. Variations in peak (u, v) for a moving group with galactic longitude could be a function of proximity to a spiral arm ridge. The gradients of mean velocity components with position in a simulated galaxy (e.g. see fig. 2 by Grand et al. 2015) seem large enough to account for the smooth variations or gradient of the highest peak which is usually labelled as the Hyades cluster. Its negative u and v values are consistent with being on the trailing side of a spiral arm. This and the proximity of the Local Arm suggest that smooth variations in v as a function of galactic longitude in the Hyades stream are caused by the Local Arm. One can choose a set of neighbourhoods, similar to those covered by the GALAH survey, but in the simulated galaxy of fig. 2 by Grand et al. (2015) and with central position lagging a spiral arm. It may be possible to choose the central position with respect to the spiral structure so that the peaks in the local velocity distributions of the simulation exhibits the near sinusoidal variation in v with galactic longitude that we see in the Hyades stream peak velocities.

Proximity to a single arm might account for variations in peak (u, v) values or of the entire velocity distribution as a function of position but would not account for the multiple peaks in the velocity distributions and how they vary with position in the Galaxy. Fine structure seen in local velocity distributions that varies over distances as short as a few hundred pc is a surprise. Strong spiral arms could cause more than one clump and deviations in the velocity distribution across short distances if there are local resonances with a spiral pattern (e.g. Quillen & Minchev 2005) or if multiple patterns are present in the disc (e.g. Quillen et al. 2011). The illustrations in fig. 11 Quillen et al. (2011) show how stars at different guiding radii and perturbed by different patterns can be present in a single neighbourhood, giving two velocity clumps in a local stellar distribution. However, previous studies (Quillen et al. 2011; Grand et al. 2015) did not expect so much substructure in the velocity distributions at lower velocities and the large gradients. Many transient spiral patterns, simultaneously in the disc, might give numerous clumps in the velocity distribution (De Simone et al. 2004) and gradients in their locations. A bar model that takes into account relaxation following bar growth and evolution also might be consistent with variations in the velocity distribution over short distances such as a few hundred pc (Minchev et al. 2010). Or perhaps there are short wavelength spiral density waves travelling through the disc, similar to those seen in self-gravitating *N*-body shearing sheet simulations (Toomre & Kalnajs 1991; Quillen et al. 2018) and these might cause substructure in local velocity distributions. Smaller scale spiral structures such as branches, spurs, feathers, and arm-segments are seen in external spiral galaxies (Sandage 1961; Lynds 1970; Elmegreen 1980), and these too may manifest as substructure in local velocity distributions if they are present in the Galactic disc near the Sun (Skuljan 1999). Up to this point we have primarily discussed dynamical mechanisms associated with perturbations to the Galactic disc. Chemically homogeneous dissolved star clusters could also contribute to the substructure in local velocity distributions.

5.2 Dependence of nearby velocity distributions on Galactic hemisphere

Following a suggestion by Agris Kalnajs, we recreated our velocity histograms for stars only at positive and negative Galactic latitudes. The velocity distributions for $d < 500$ pc were not significantly sensitive to the Galactic hemisphere, so we again only show distributions for the $d < 250$ pc stars. Velocity distributions for both hemispheres in the high metallicity, near solar and lower metallicity samples and for $d < 250$ pc, are shown in Figs 10–12. We were surprised to find that the Hyades and Sirus/UMa groups are predominantly seen at galactic latitudes $b > 0°$ for $d < 250$ pc near solar and lower metallicity stars. The Coma Berenices group is predominantly seen at galactic latitudes $b < 0°$ and on the opposite side as the Coma Berenices open cluster itself which is seen near the Galactic north pole. We confirm the prior discovery by Agris Kalnajs (private communication) found previously using *Hipparcos* proper motions.

The dependence of peak positions in the velocity distribution on Galactic hemisphere is unexpected. Possible causes include small number statistics, as the GALAH sample is not uniformly distributed across the sky. There could be variations in the distance distributions along different sightlines. If the peak velocities depend on distance from the Sun, then variations in the distance distributions could cause variations in these peak velocities along different sightlines. Alternatively, if there really is small-scale structure in the velocity distributions and strong gradients in the velocity distributions within the Galaxy, we would expect correlated stellar density variations. In other words, we should also see changes in the number density of stars or stars per unit volume in the Galaxy. There may also be correlated vertical velocity variations. Correlated variations in stellar number density and vertical motions are predicted if correlated vertical and radial epicyclic motions in the disc are induced by perturbations from dwarf galaxies in the outer Galaxy (de la Vega et al. 2015) or vertical breathing and bending waves travel through the disc (Widrow et al. 2012, 2014; Widrow & Bonner 2015).

To investigate the effect of uneven sky coverage and to see if there are sightline-dependent differences in the distance distributions, we plot the distance distributions for nearby GALAH stars in Fig. 13. Our histograms count stars in bins that are 10 pc wide in distance and

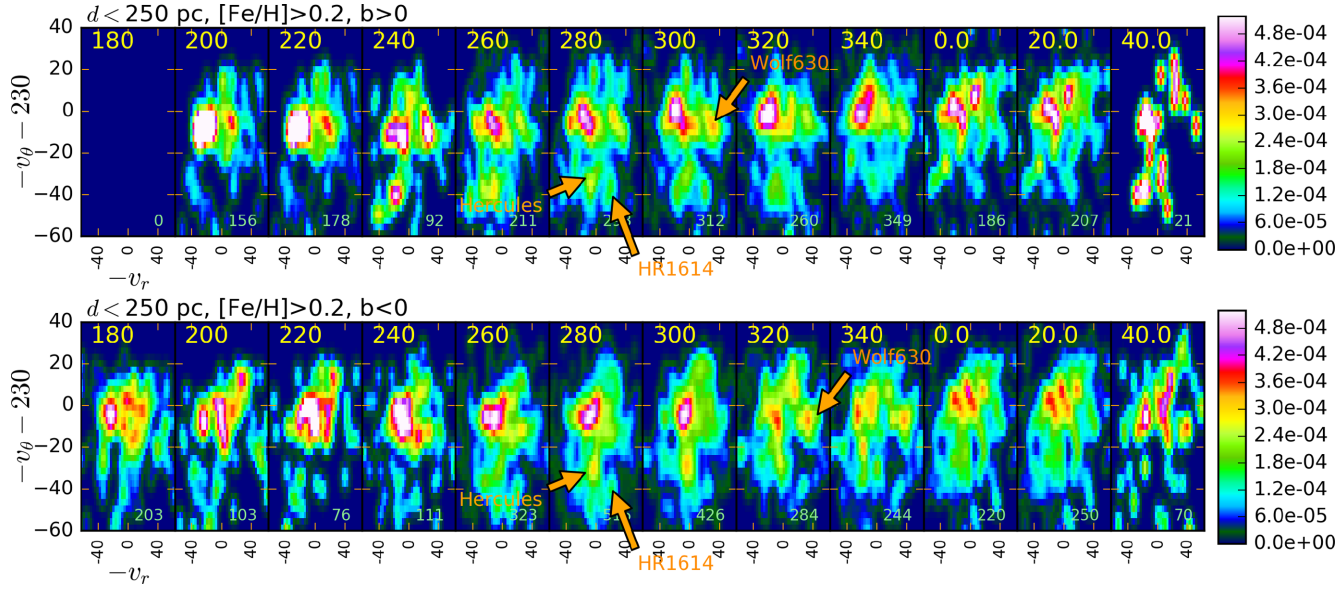

Figure 10. Velocity distributions in uv similar to those shown in Fig. 6(a) for high-metallicity stars, but restricted to positive (top panel) and negative (bottom panel) galactic latitudes.

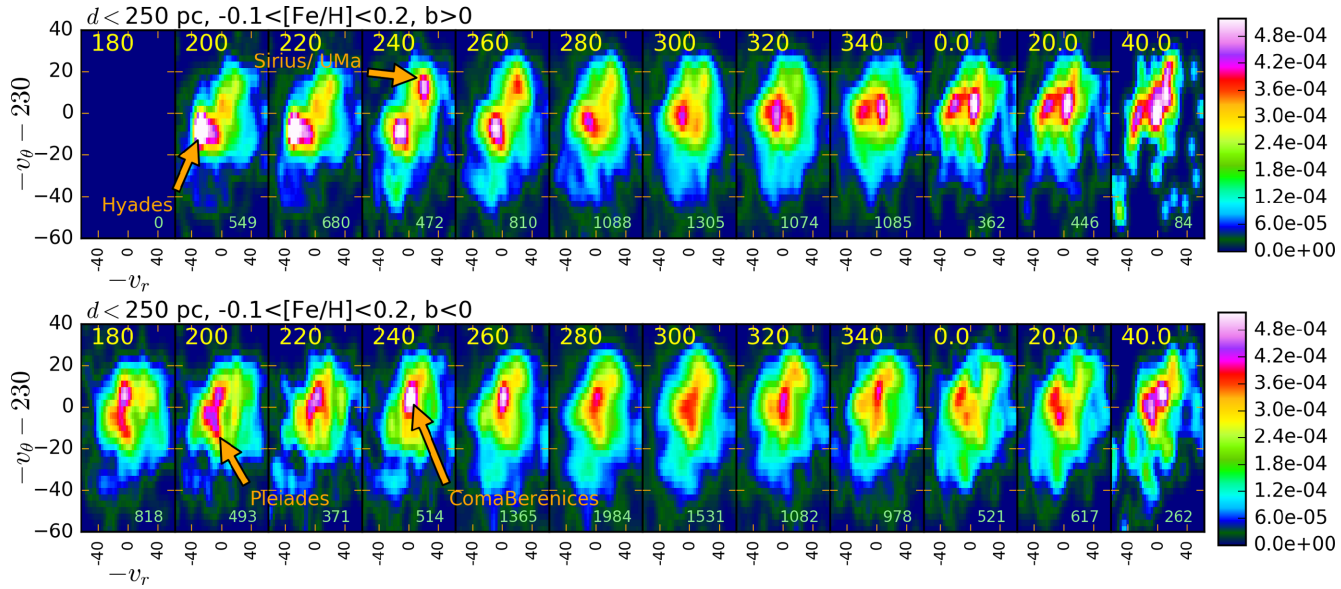

Figure 11. Velocity distributions in uv similar to those shown in Fig. 6(b) for near solar metallicity stars, but restricted to positive (top panel) and negative (bottom panel) galactic latitudes.

4° wide in galactic longitude. The axes for distance are shown on the left in pc. The bottom axes show galactic longitude ℓ in degrees. The histograms have been normalized so that each column, specified by its galactic longitude, sums to 1. The normalization makes it easier to compare distance distributions at different longitudes. The colourbars show the fraction of stars (at each longitude) that is present in each 10 pc wide bin. The total numbers of stars with $d < 250$ pc in each galactic longitude bin is plotted as a white and black line with y-axis on the right showing the scale. Top panels show stars in the northern Galactic hemisphere (with Galactic latitude $b > 0°$), middle panels shows stars in the southern Galactic hemisphere, and the bottom panels show stars in both hemispheres. Three sets of histograms are shown. On the left, we show the high-metallicity stars with [Fe/H] > 0.2. The middle panels show near solar metallicity stars ($-0.1 <$ [Fe/H] < 0.2) and the right panels show low-metallicity stars ([Fe/H] < -0.1). As before, only stars at latitudes $|b| < 45°$ and with distance errors $\sigma_d/d < 0.5$ are used to construct the histograms.

The distance histograms in Fig. 13 show that the low-metallicity GALAH stars have the largest variations in distance distribution between hemispheres. The region in galactic longitude with $200° < \ell < 260°$ has a ridge at $d \sim 130$ pc in the southern Galactic hemisphere that is absent in the northern Galactic hemisphere. The number density variations are strongest where there are fewest stars, which is a concern. Stars 130 pc away from the Sun and along $\ell \sim 230°$ could tend to have velocity vector like the Coma Berenices group. However, the distance distribution in the near solar metallicity stars do not show as large hemisphere sensitive variations as

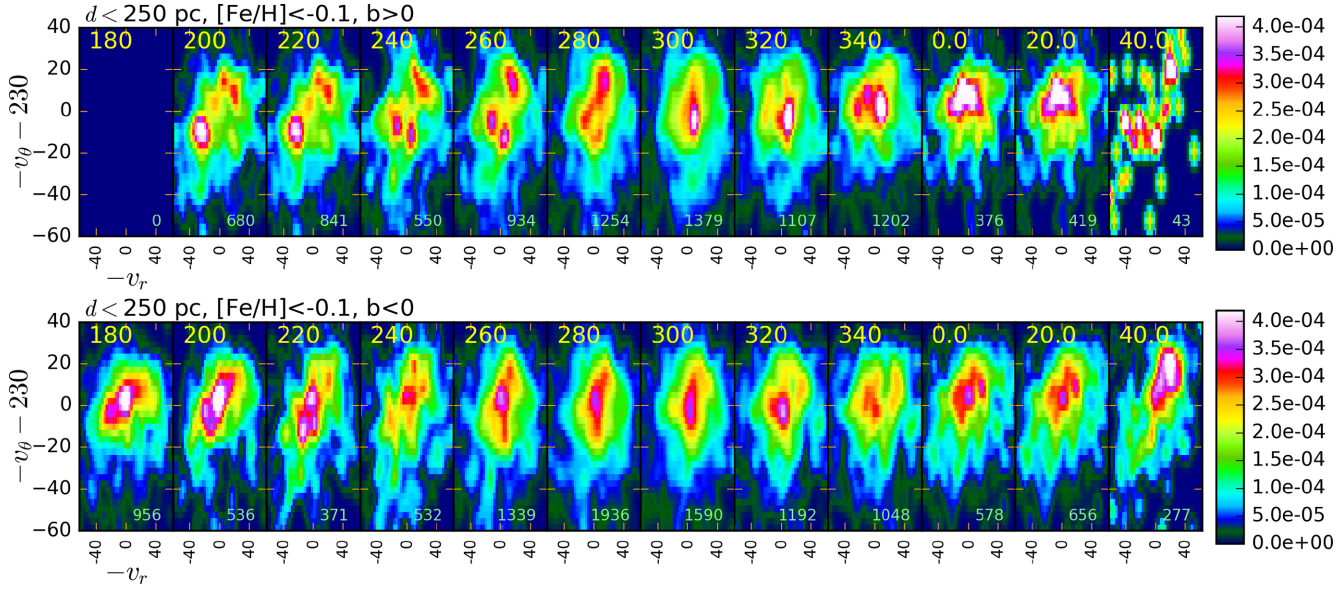

Figure 12. Velocity distributions in *uv* similar to those shown in Fig. 6(c) for low-metallicity stars, but restricted to positive (top panel) and negative (bottom panel) Galactic latitudes. The velocity distributions of low-metallicity stars are the most sensitive to Galactic hemisphere, with Coma Berenices moving group preferentially seen in the southern Galactic hemisphere and Hyades and Sirius/UMa groups preferentially seen in the northern Galactic hemisphere.

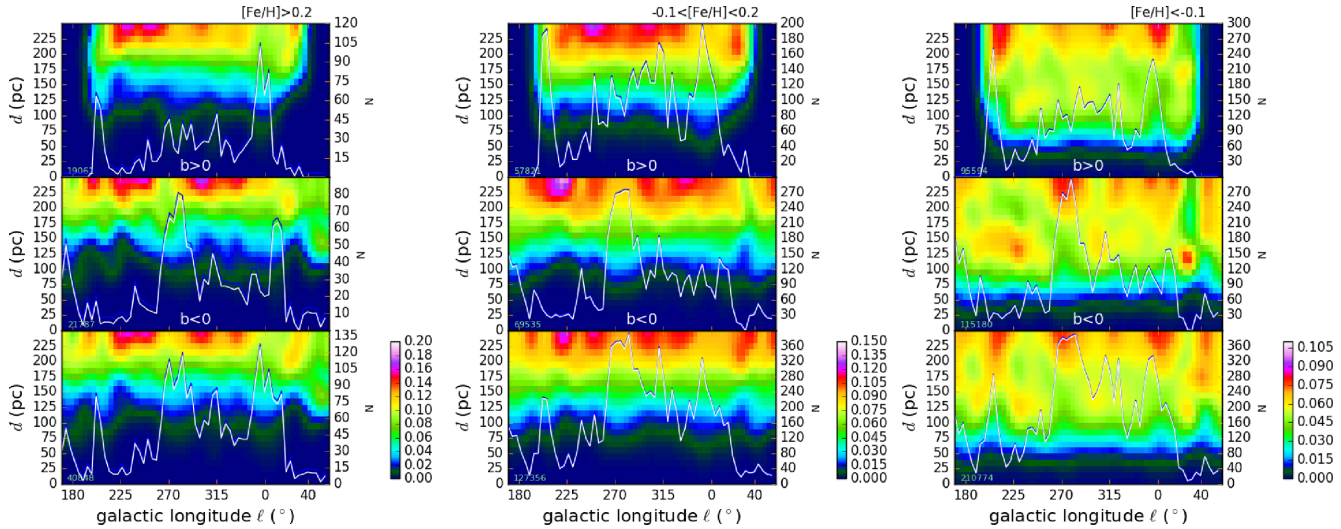

Figure 13. Distance distributions of the GALAH sample as a function of galactic longitude and for the three different metallicity sets, with high metallicity on the left, near solar metallicity in the middle and lower metallicity on the right. Each panel shows a histogram showing numbers of stars in distance and galactic longitude bins. The histograms have been normalized so that each column, specified by its galactic longitude, sums to 1. The colourbars show the fraction of stars at a given longitude per 10 pc wide bin in distance. Distance axis is on the left and the galactic longitude axis is on the bottom. Galactic longitude bins are 4° wide. The total numbers of stars at each galactic longitude is plotted as a white line with *y*-axis showing the scale on the right. Top panels refer to stars in the northern Galactic hemisphere with Galactic latitude $b > 0°$, the middle panels for stars in the southern Galactic hemisphere, and the bottom panels for stars in both hemispheres. Only the low-metallicity stars show large differences in the distance distributions between hemispheres.

the low-metallicity stars. After removing the stars within 130 pc, we still see the Coma Berenices stream in the Southern hemisphere velocity distribution in near solar metallicity stars, so this stream is not confined to very nearby stars.

In the previous section, we inferred that there was evidence for variations in the velocity distributions (in *u*, *v*) over short distances. Variations or gradients in the velocity distributions, if they are real, probably would be associated with density variations (variations in the number of stars per unit volume) over similar spatial scales. It is tempting to interpret the differences in the distance distributions in Fig. 13 and in the lower metallicity stars as evidence for variations in stellar number density. However, no similar density variations are seen in the near solar metallicity stars and they too show the asymmetry in the velocity distributions for $200° < \ell < 260°$.

At a distance of 200 pc, a star that has galactic latitude $b = 10°$ (the latitude limit of the GALAH survey) is 34 pc above the Galactic plane (where we have ignored the Sun's offset), and that at $b = 45°$ is 143 pc above the plane, but still within the thin disc scale height. The differences in velocities seen between the northern and southern Galactic hemispheres correspond to a vertical gradient in *v*

component velocity of about $10\,\mathrm{km\,s^{-1}}$ across 300 pc (approximately multiplying 134 by 2) corresponding to about $30\,\mathrm{km\,s^{-1}\,kpc^{-1}}$. This is similar in size to the gradient in the plane we estimated for peaks in (u, v).

Does the position of the Sun, 25 ± 5 pc (see Bland-Hawthorn & Gerhard 2016 for a review of recent measurements), above the plane in the Galactic north pole direction, account for the differences in peak velocities seen in the two Galactic hemispheres? Taking into account a 25 pc offset for the Sun, a star at 200 pc and at $b = 10^\circ$, $-10^\circ, 45^\circ, -45^\circ$ would be at $z = 9, -59, 118, -159$ pc, respectively. These values lie well within the thin disc. Strong vertical velocity gradients in the thin disc would still be required for the position of the Sun above the Galactic plane to affect the viewed velocity distributions.

Vertical gradients in the (u, v) velocity distributions, if they are real, probably would be associated with vertical velocity variations. To test this possibility, we examine velocity distributions in (v, w) with $w = v_z$ the vertical velocity component. Fig. 14 shows (v, w) velocity distributions for nearby ($d < 250$ pc), near solar metallicity stars ($-0, 1 <$ [Fe/H] < 0.2) that are in the north Galactic hemisphere and that are in the Southern hemisphere, separately. Histograms are shown with w on the x-axis and v on the y-axis (top two panels) and vice versa for in bottom two panels. The first and third panels show northern Galactic hemisphere, and the second and forth panels (from top) show the southern Galactic hemisphere. Fig. 14 shows that the w values of velocity peaks are dependent on Galactic longitude and on hemisphere. For example, we compare the $\ell = 260^\circ$ histograms. For $b > 0$ the largest clump (associated with the Hyades group) has $w \sim 3\mathrm{km\,s^{-1}}$, whereas for $b < 0$ the largest clump (with the Coma Berenices group) has $w \sim -3\,\mathrm{km\,s^{-1}}$. These deviations are near but above our estimated precision of about $1\,\mathrm{km\,s^{-1}}$. The variations in peak velocities are shown as a function of Galactic longitude in Fig. 15. This figure is similar to Fig. 9 except circles show peaks from the velocity distributions in the northern Galactic hemisphere (and identified in the velocity distributions of Fig. 14, top panel) and squares show the northern Galactic hemisphere (and identified in the velocity distributions of Fig. 14, bottom panel).

A single neighbourhood can contain more than one velocity peak if there are correlations in both vertical epicyclic and radial epicyclic phases. Stars coming into the neighbourhood from the outer Galaxy could be at different phases in the vertical oscillations than stars moving outwards from the inner Galaxy (see de la Vega et al. 2015). If the thin disc has a scale height of 300 pc and a vertical dispersion of $20\,\mathrm{km\,s^{-1}}$ (taking typical values from Bland-Hawthorn & Gerhard 2016), a vertical velocity of $w = 3\,\mathrm{km\,s^{-1}}$ would allow a star to reach about 45 pc above the Galactic plane. This is high enough that the star might be seen in one hemisphere and not the other. In other words, the sizes of the vertical velocity variations are approximately consistent with the extent of vertical motions that would allow differences in the velocity distributions to be seen above and below the Galactic plane.

In summary, we find that the Coma Berenices group is predominantly seen at galactic longitude $l \sim 230^\circ$,at galactic latitude $b < 0$, and in solar and low-metallicity stars. The Hyades and Sirius/UMa groups are more prominent at positive galactic latitude in the same metallicity range and longitudes. The variations in velocity peak velocities in the velocity distributions with Galactic hemisphere are not clearly associated with variations in the stellar distance distributions but may be correlated with $\sim 3\,\mathrm{km\,s^{-1}}$ variations in peak vertical velocities w. Such correlations are predicted if the Galactic disc hosts vertical breathing and bending waves (Widrow et al. 2012, 2014; Widrow & Bonner 2015) or exhibits correlated phases in vertical and radial epicyclic motions caused by perturbations in the outer Galaxy (de la Vega et al. 2015). However, asymmetries (with hemisphere) in both number density and velocity distribution are largest, where there are fewest GALAH stars so the differences in the velocity distributions with direction on the sky may be due to statistical variations. Larger samples of stars are needed to see if the correlated variations in peak velocities in local velocity distributions are real.

6 SUMMARY AND CONCLUSION

We have used GALAH survey data to construct local velocity distributions at neighbourhoods near the Sun but comprised of stars seen at different galactic longitudes. We find that the Hercules stream is most prominent in nearby high-metallicity stars, with [Fe/H] > 0.2, (confirming the works by Liu et al. 2015; Liu 2016; Perez-Villegas et al. 2017), but is also present in solar-metallicity stars ($-0.1 <$ [Fe/H] < 0.2), and difficult to see in metal-poor stars with ([Fe/H] < -0.1). An extension to low v overlaying the Hercules stream is also seen in high-α-element stars. The dependence of the Hercules stream on metallicity is not surprising as metallicity distributions at smaller galactocentric radii contain more metal-rich stars (e.g. Hayden et al. 2015).

We find that a gap in the velocity distributions between the Hercules stream and stars in more nearly circular orbits is approximately at an angular momentum value of $L_{\mathrm{gap}} \approx 1640 \pm 40\,\mathrm{km\,s^{-1}}$ kpc. The gap is seen in a histogram of angular momentum versus orbital eccentricity and is consistent with v gap values in the local velocity distributions for neighbourhoods of stars observed at different galactic longitudes. The association of the Hercules stream with a particular angular momentum value supports a bar resonant model as the angular momentum sets the period of orbits and so determines those that are resonant with the bar pattern speed. The value we estimate for L_{gap} is consistent with that of the Outer Lindblad Resonance for a fast and short bar model (Dehnen 2000; Minchev et al. 2007; Antoja et al. 2014; Monari et al. 2017; Hunt et al. 2018), but $300\,\mathrm{km\,s^{-1}}$kpc above that of corotation for the slow and long bar model (that by Perez-Villegas et al. 2017 and Portail et al. 2017a).

When we construct velocity distributions for nearer stars with distance $d < 250$ pc, we recover peaks in the velocity distributions at locations of moving groups seen previously in *Hipparcos* observations. However, the location of these peaks varies as a function of metallicity, viewed galactic longitude, and whether viewed in the northern or southern Galactic hemispheres (positive or negative galactic latitudes). We infer that structures in the velocity distribution varies over distances as short as a few hundred pc in the Galactic disc. Gradients in peak velocities have size of order $25\,\mathrm{km\,s^{-1}\,kpc^{-1}}$, corresponding to changes of $10\,\mathrm{km\,s^{-1}}$ across 400 pc. The variations over distances this short is unexpected. Possible causes are streaming associated with multiple spiral density waves, dissolved clusters, resonances with bar or spiral patterns, or small scale spiral features such as feathers, branches, arm-segments or spurs. We see differences in the uv positions of velocity peaks between the two Galactic hemispheres that may be correlated with $\sim 3\,\mathrm{km\,s^{-1}}$ variations in vertical velocity component w. Possible causes are vertical breathing and bending waves (Widrow et al. 2012, 2014; Widrow & Bonner 2015) or correlated phases in epicyclic motions caused by perturbations in the outer Galaxy (de la Vega et al. 2015). Unfortunately, we see these variations at galactic longitudes where

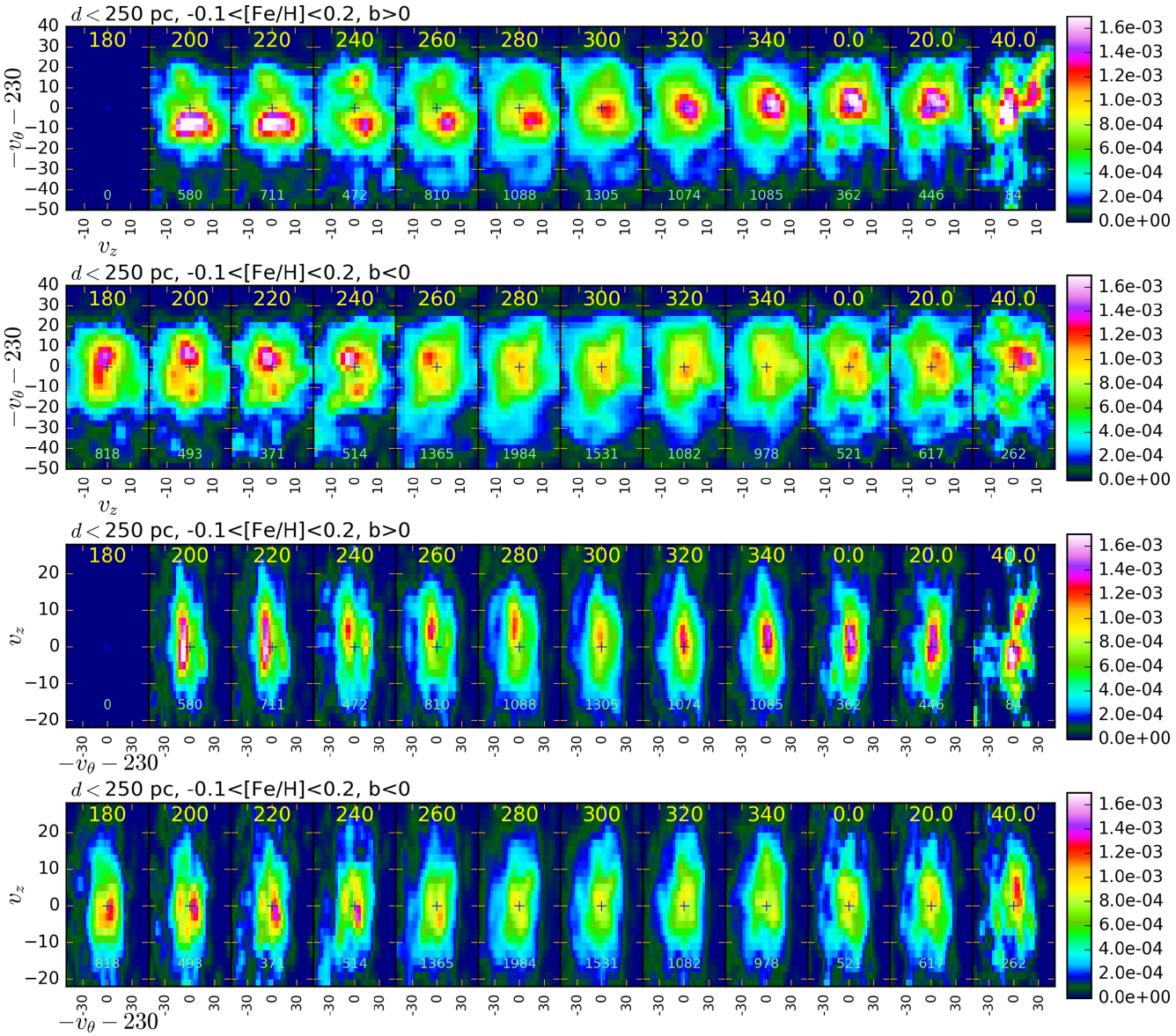

Figure 14. Velocity distributions in v, w for near solar metallicity stars. The x-axes in the top and second from top panels are v and y-axes are w. The third from top and bottom panels are reversed with x-axes w and y-axes v. The top and third from top panels show stars in the northern Galactic hemisphere (latitude $b > 0$),whereas the second from top and bottom panels show stars in the northern Galactic hemisphere.

we have the fewest GALAH stars and so suspect that small number statistics could have given us spurious peaks in our normalized histograms.

The velocity distributions we constructed for more distant stars (within 500 pc) failed to show as much substructure as the nearby stars (within 250 pc). This could be due to coarse graining caused by using a larger volume to count stars or due to larger errors in the distances and space motions that are present in the more distant stars. The velocity distributions may depend on height from the Galactic plane and may be biased by differences in the numbers of stars present in the survey along the different sightlines. The GALAH survey stars are predominantly less than 1 kpc away. Future studies with higher precision at greater distances will determine if substructure in local velocity distributions exists in other regions in the Galaxy and if it varies over short distances, as found here. By studying in more detail the abundances (chemical tagging; De Silva et al. 2007; Bland-Hawthorn et al. 2010; Mitschang et al. 2014; Ting, Conroy & Rix 2016) using age indicators (such as chromospherically sensitive lines; Žerjal et al. 2017) and studying larger and more uniformly distributed samples, we may differentiate between causative dynamical mechanisms.

GALAH targets have a well-defined magnitude distribution. A problem with a sample chosen with a narrow magnitude range is that more distant stars tend to have higher luminosities. We have neglected this distance-dependent difference in the stellar distributions, as we have no reason to think this would significantly impact the velocity or metallicity distributions. We have not attempted to take into account how extinction affects the distributions of stars in the sample. Future attempts to characterize and compare local velocity distributions outside the solar neighbourhood, at higher precision and at larger distances from the Sun, may need to consider how variations in the sampled local stellar distributions affect the local velocity and metallicity distributions.

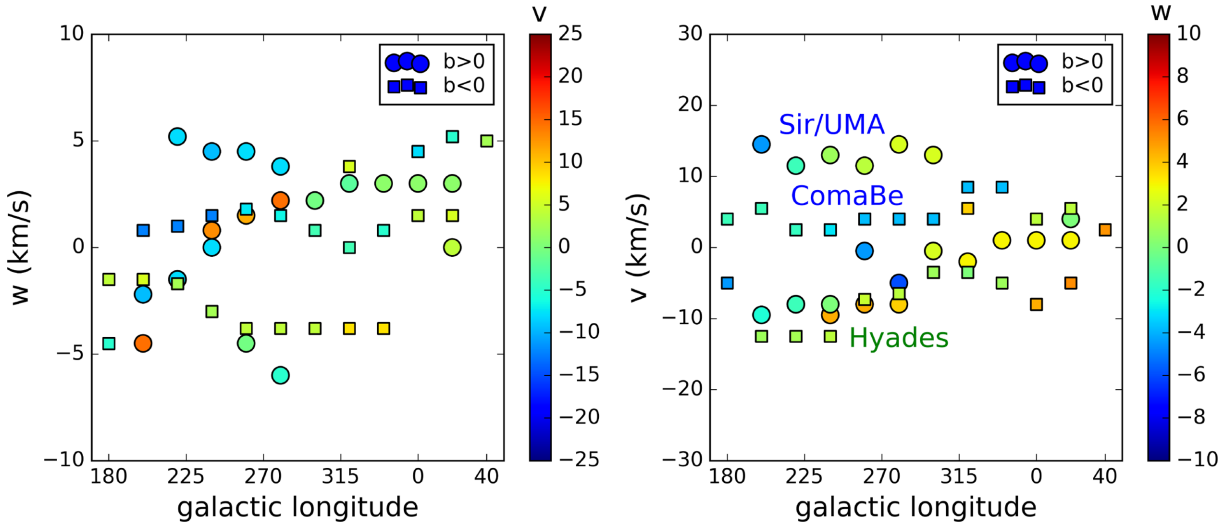

Figure 15. Peaks seen in the $d > 250$ pc (v, w) velocity distributions of near solar metallicity stars in Fig. 14 have $w = v_z$ velocity component plotted as a function of galactic longitude in the left-hand panel. The colour of the points depends on the v velocity (with $v = -v_\theta - 230\,\mathrm{km\,s^{-1}}$, as before). In the right-hand panel, the peak v velocity is plotted as a function of galactic longitude and with colour set by the w velocity. Sirius/UMa, Coma Berenices, and Hyades, streams or moving groups are most easily identified in the panel on the right where they are labelled. This figure is similar to Fig. 9 expect round points show the northern Galactic hemisphere (galactic latitude $b > 0$) and square points show the southern Galactic hemisphere. The Coma Berenices group is seen in the southern Galactic hemisphere, whereas the Sirius/UMa group is seen in the northern Galactic hemisphere. The peak w velocities of each group varies as a function of galactic longitude and Galactic hemisphere. Smooth variations in w with longitude are most easily seen in the right-hand panel.

ACKNOWLEDGEMENTS

ACQ thanks Mt. Stromlo Observatory for their warm welcome and hospitality 2017 November–2018 February. ACQ is grateful to the Leibniz Institut für Astrophysik Potsdam for their warm welcome, support, and hospitality 2017 July and 2018 May. ACQ is pleased to be a Visiting Scholar associated with the Hunstead Gift for Astrophysics to the University of Sydney. ACQ is grateful for generous support from the Simons Foundation and her work is in part supported by NASA grant 80NSSC17K0771. We thank Agris Kalnajs for helpful and critical discussions. Without his suggestion, we would not have found the results presented in Section 5.2.

Parts of this research were conducted by the Australian Research Council (ARC) Centre of Excellence for All Sky Astrophysics in 3 Dimensions (ASTRO 3D), through project number CE170100013. JB-H acknowledges a Miller Professorship from the Miller Institute, UC Berkeley, and an ARC Laureate Fellowship which also supports GDS and SS. SM acknowledges support from the ARC through DECRA Fellowship DE140100598. JK is supported by an ARC DP grant awarded to JB-H and TB. MH is supported by ASTRO 3D Centre of Excellence funding to the University of Sydney and an ARC DP grant awarded to KF. LD gratefully acknowledges a scholarship from Zonta International District 24. LD and KF acknowledge support from ARC grant DP160103747. LC is the recipient of an ARC Future Fellowship (project number FT160100402).

We acknowledge support of the Slovenian Research Agency (research core funding No. P1-0188). DMN was supported by the Allan C. and Dorothy H. Davis Fellowship. Y-ST is supported by the Carnegie-Princeton Fellowship and the Martin A. and Helen Chooljian Membership from the Institute for Advanced Study in Princeton.

This work is based on data acquired through the Australian Astronomical Observatory, under programmes: A/2013B/13 (The GALAH pilot survey); A/2014A/25, A/2015A/19, A2017A/18 (The GALAH survey); A/2015A/03, A/2015B/19, A/2016A/22, A/2016B/12, A/2017A/14 (The K2-HERMES K2-follow-up programme); A/2016B/10 (The HERMES-TESS programme); A/2015B/01 (Accurate physical parameters of Kepler K2 planet search targets); and S/2015A/012 (Planets in clusters with K2).

REFERENCES

Adibekyan V. Z., Sousa S. G., Santos N. C., Delgado Mena E., Gonzalez Hernandez J. I., Israelian G., Mayor M., Khachatryan G., 2012, A&A, 545, A32
Anders F. et al., 2017, A&A, 600, A70
Anguiano B., Majewski S. R., Freeman K. C., Mitschang A. W., Smith M. C., 2018, MNRAS, 474, 854
Antoja T. et al., 2014, A&A, 563, A60
Antoja T. et al., 2015, ApJ, 800, L32
Badenes C. et al., 2018, ApJ, 854, 147
Baumgardt H., Makino J., 2003, MNRAS, 340, 227
Bensby T., Feltzing S., Lundstrom I., 2003, A&A, 410, 527
Bensby T., Oey M. S., Feltzing S., Gustafsson B., 2007a, ApJ, 655, L89
Bensby T., Zenn A. R., Oey M. S., Feltzing S., 2007b, ApJ, 663, L13
Bensby T., Feltzing S., Oey M. S., 2014, A&A, 562, A71
Bland-Hawthorn J., Gerhard O., 2016, ARA&A, 54, 529
Bland-Hawthorn J., Krumholz M. R., Freeman K., 2010, ApJ, 713, 166
Bovy J., Hogg D. W., 2010, ApJ, 717, 617
Bubar E. J., King J. R., 2010, AJ, 140, 293
Buder S. et al., 2018, MNRAS, preprint, arxiv.org/abs/1804.06041
Carlin J. L. et al., 2013, ApJ, 777, L5
Carrillo I. et al., 2018, MNRAS, in press, arxiv.org/abs/1710.03763
Casagrande L., Schoenrich R., Asplund M., Cassisi S., Ramirez I., Melendez J., Bensby T., Feltzing S., 2011, A&A, 530, 138
Chakrabarty D., Sideris I. V., 2008, A&A, 488, 161
Contopoulos G., 1975, ApJ, 201, 566
de la Vega A., Quillen A. C., Carlin J. L., Chakrabarti S., D'Onghia E., 2015, MNRAS, 454, 933
De Silva G., Freeman K. C., Bland Hawthorn J., Asplund M., Bessel M. S., 2007, AJ, 133, 694
De Silva G. M., Freeman K. C., Bland-Hawthorn J., Asplund M., Williams M., Holmberg J., 2011, MNRAS, 415, 563
De Silva G. et al., 2015, MNRAS, 449, 2604

De Simone R., Wu X., Tremaine S., 2004, MNRAS, 350, 627
Dehnen W., 1998, AJ, 115, 2384
Dehnen W., 1999a, AJ, 118, 1190
Dehnen W., 1999b, ApJ, 524, L35
Dehnen W., 2000, AJ, 119, 800
Duong L. et al., 2018, MNRAS, 476, 5216
Eggen O. J., 1958a, MNRAS, 118, 65
Eggen O. J., 1958b, MNRAS, 118, 154
Eggen O. J., 1958c, MNRAS, 118, 560
Eggen O. J., 1965a, Observatory, 85, 191
Eggen O. J., 1965b, Observatory, 85, 104
Eggen O. J., 1965c, in Blaauw A., Schmidt M., eds, Stars and Stellar Systems, Vol. 5, Galactic Structure. Univ. Chicago Press, Chicago, p. 111
Eggen O. J., 1970, PASP, 82, 99
Eggen O. J., 1995, AJ, 111, 1615
Eggen O. J., 1996, AJ, 112, 1595
Eggen O. J., 1998, AJ, 115, 2453
El-Badry K. et al., 2018, MNRAS, 477, 1536
Elmegreen D. M., 1980, ApJ, 242, 52
Famaey B., Jorissen A., Luri X., Mayor M., Udry S., Dejonghe H., Turon C., 2005, A&A, 430, 165
Freeman K., Bland-Hawthorn J., 2002, ARA&A, 40, 487
Fuchs B., 2001, A&A, 368, 107
Fuhrmann K., 1998, A&A, 338, 161
Fujii M. S., Portugies Zwart S., 2016, ApJ, 817, 4
Fux R., 2001, A&A, 373, 511
Gardner E., Flynn C., 2010, MNRAS, 405, 545
Gilmore G. et al., 2012, Messenger, 147, 25
Grand R. J. J., Kawata D., Cropper M., 2014, MNRAS, 439, 623
Grand R. J. J., Bovy J., Kawata D., Hunt J. A. S., Famaey B., Siebert A., Monari G., Cropper M., 2015, MNRAS, 453, 1867
Hayden M. R. et al., 2015, ApJ, 808, 132
Hayden M. R. et al., 2018, A&A, 609, 79
Holmberg J., Nordström B., Andersen J., 2009, A&A, 501, 941
Hou L. G., Han G. L., 2014, A&A, 569, A125
Hunt J. A. S. et al., 2018, MNRAS, 474, 95
Kalnajs A. J., 1991, in Sundelius B., ed., Dynamics of Disc Galaxies, Proc. Conf. Varberg Castle, Sweden, p. 323
Kapteyn J. C., 1905, Br. Assoc. Rep., p. 207
King J. R., Schuler S. C., 2005, PASP, 117, 911
Kos J. et al., 2017, MNRAS, 464, 1259
Kos J. et al., 2018, MNRAS, 473, 4612
Lepine J. R. D., Roman-Lopes A., Abraham Z., Junqueira T. C., Mishurov Y. N., 2011, MNRAS, 414, 1607
Lewis I. J. et al., 2002, MNRAS, 333, 279
Liang X. L., Zhao J. K., Oswalt T. D., Chen Y. Q., Zhang L., Zhao G., 2017, ApJ, 844, 152
Liu C., 2016, in Conf. Galact. Archaeol. Stellar Phys., https://www.aao.gov.au/conference/gasp16
Liu C. et al., 2015, https://arxiv.org/abs/1510.06123
Lynds B. T., 1970, in Becker W., Contopoulos G. I., eds, IAU Symp. 38, The Spiral Structure of Our Galaxy. Dordrecht, Reidel, p. 38
Majewski S. R. et al., 2015, eprint, https://arxiv.org/abs/1509.05420
Martell S. L. et al., 2017, MNRAS, 465, 3203
Michalik D., Lindegren L., Hobbs D., 2015, A&A, 574, A115
Minchev I., Nordhaus J., Quillen A. C., 2007, ApJ, 664, L31
Minchev I., Boily C., Siebert A., Bienayme O., 2010, MNRAS, 407, 2122
Mitschang A. W., De Silva G., Zucker D. B., Anguiano B., Bensby T., Feltzing S., 2014, MNRAS, 438, 2753
Monari G., Kawata D., Hunt J. A. S., Famaey B., 2017, MNRAS, 466, L113
Ness M., Hogg D. W., Rix H.-W., Ho A. Y. Q., Zasowski G., 2015, ApJ, 808, 16
Oort J. H., Kerr F. J., Westerhout G., 1958, MNRAS, 118, 379
Pearl A. N., Newberg H. J., Carlin J. L., Smith R. F., 2017, ApJ, 847, 123
Perez-Villegas A., Portail M., Wegg C., Gerhard O., 2017, ApJ, 840, L2
Perryman M. A. C. et al., 1997, A&A, 323, L49
Pompeia L. et al., 2011, MNRAS, 415, 1138
Portail M., Gerhard O., Wegg C., Ness M., 2017a, MNRAS, 465, 1621
Portail M., Wegg C., Gerhard O., Ness M., 2017b, MNRAS, 470, 1233
Quillen A. C., 2003, AJ, 125, 785
Quillen A. C., Minchev I., 2005, AJ, 130, 576
Quillen A. C., Minchev I., Bland-Hawthorn J., Haywood M., 2009, MNRAS, 397, 1599
Quillen A. C., Dougherty J., Bagley M. B., Minchev I., Comparetta J., 2011, MNRAS, 417, 762
Quillen A. C., Minchev I., Sharma S., Qin Y.-J., Di Matteo P., 2014, MNRAS, 437, 1284
Quillen A. C., Nolting E., Minchev I., De Silva G., Chiappini C., 2018, MNRAS, 475, 4450
Raboud D., Grenon M., Martinet L., Fux R., Udry S., 1998, A&A, 335, L61
Ramya P., Reddy B. E., Lambert D. L., Musthafa M. M., 2016, MNRAS, 460, 1356
Randich S. et al., 2013, Messenger, 154, 47
Reid M. J., 1993, ARA&A, 31, 345
Reid M. J., Brunthaler A., 2004, ApJ, 616, 872
Robin A. C., Bienayme O., Fernandez-Trincado J. G., Reyle C., 2017, A&A, 605, A1
Russeil D., 2003, A&A, 397, 133
Sandage A., 1961, The Hubble Atlas of Galaxies, Carnegie Institution, Washington DC
Schönrich R., Binney J., Dehnen W., 2010, MNRAS, 403, 1829
Schwarschild K., 1907, Gotting. Nach, 5, 614
Sharma S. et al., 2014, ApJ, 793, 51
Sharma S. et al., 2018, MNRAS, 473, 2004
Sheinis A. et al., 2015, J. Astron. Telesc. Instrum. Syst., 1, 035002
Siebert A. et al., 2011, MNRAS, 412, 2026
Skrutskie M. F. et al., 2006, AJ, 131, 1163
Skuljan J., 1999, PhD thesis. Univ. Canterbury, http://hdl.handle.net/10092/5579
Skuljan J., Hearnshaw J. B., Cottrell P. L., 1999, MNRAS, 308, 731
Steinmetz M. et al., 2006, AJ, 132, 1645
Sun N.-C. et al., 2015, Res. Astron. Astrophys., 15, 1342
Tabernero H. M., Montes D., González Hernández J. I., 2012, A&A, 547, A13
Tabernero H. M., Montes D., González Hernández J. I., Ammler-von Eiff M., 2017, A&A, 597, A33
Ting Y.-S., Conroy C., Rix H.-W., 2016, ApJ, 816, 10
Toomre A., Kalnajs A. J., 1991, in Sundelius B., ed., Dynamics of Disc Galaxies. Göteborg, Sweden, p. 341.
Vazquez R. A., May J., Carraro G., Bronfman L., Moitinho A., Baume G., 2008, ApJ, 672, 930
Weinberg M. D., 1994, ApJ, 420, 597
Widrow L. M., Bonner G., 2015, MNRAS, 450, 266
Widrow L. M., Gardner S., Yanny B., Dodelson S., Chen H.-Y., 2012, ApJ, 750, L41
Widrow L. M., Barber J., Chequers M. H., Cheng E., 2014, MNRAS, 440, 1971
Williams M. E. K. et al., 2013, MNRAS, 436, 101
Wilson G. A., 1990, PhD thesis, Australian National University
Wittenmyer R. et al., 2018, AJ, 155, 84
Wojno J. et al., 2017, MNRAS, 468, 3368
Xu Y. et al., 2013, ApJ, 769, 15
Xu Y., Newberg H. J., Carlin J. L., Liu C., Deng L., Li J., Schonrich R., Yanny B., 2015, ApJ, 801, 105
Xu Y. et al., 2016, Sci. Adv., 2, e160087
Yanny B. et al., 2009, AJ, 137, 4377
Zacharias N., Finch C. T., Frouard J., 2017, AJ, 153, 166
Zhao G., Zhao Y.-H., Chu Y.-Q., Jing Y.-P., Deng L.-C., 2012, Res. Astron. Astrophys., 12, 723
Žerjal M. et al., 2017, ApJ, 835, 61

APPENDIX A: EPICYCLIC MOTION

Taking into account motions in the galactic plane only, the energy per unit mass of a star

$$E = \frac{v_r^2}{2} + \frac{v_\theta^2}{2} + v_c^2 \ln \frac{r}{R_\odot}, \tag{A1}$$

where we have assumed a flat rotation curve with velocity v_c and neglected bar and spiral arm perturbations in the gravitational potential. A constant offset to the energy is chosen so a circular orbit with radius $R_\odot$ has energy $E = v_c^2/2$. The z-component of angular momentum per unit mass of a star is

$$L = r v_\theta, \tag{A2}$$

where r is the star's galactocentric radius and v_θ the tangential velocity component.

Following Quillen et al. (2014, also see Fuchs 2001 and Contopoulos 1975), a Hamiltonian describing planar motion in an axisymmetric galaxy in action angle variables is

$$H(L, \theta, J, \varphi) = E_c(L) + \kappa(L) J \tag{A3}$$

to first order in epicyclic action variable J. The function $E_c(L)$ was used by Dehnen (1999a) in the development of an accurate low-order epicyclic approximation. Here, the angular momentum L is canonically conjugate to the azimuthal angle θ and the radial action variable J is conjugate to the epicyclic angle φ. The function $E_c(L)$ gives the angular rotation rate $\Omega(L)$ for a circular orbit via Hamilton's equation, or

$$\dot{\theta} = \Omega(L) = \frac{\partial H}{\partial L}(J = 0) = \frac{\partial E_c(L)}{\partial L}. \tag{A4}$$

The frequency $\kappa(L)$ is the epicyclic frequency of a nearly circular orbit with angular momentum L.

A circular orbit with angular momentum L has radius $r_c(L)$. Epicyclic oscillations are related to the radial action angle variables

$$r = r_c(L) + \sqrt{\frac{2J}{\kappa(L)}} \cos\varphi, \tag{A5}$$

$$\dot{r} = -\sqrt{2J\kappa(L)} \sin\varphi, \tag{A6}$$

$$\dot{\varphi} = \kappa(L). \tag{A7}$$

This convention for epicyclic angle gives apocentre at $\varphi = 0$, pericentre at $\varphi = \pi$, radial velocity $v_r < 0$ at $\varphi = \pi/2$, and $v_r > 0$ at $\varpi = -\pi/2$. The Hercules stream with positive v_r would have epicyclic angle $-\pi/2 < \varphi < 0$. The Hercules stream has stars that have just passed their pericentre and are moving towards apocentre. From equation (A5), we can define an orbital eccentricity

$$e \equiv \frac{1}{r_c(L)} \sqrt{\frac{2J}{\kappa(L)}}. \tag{A8}$$

For a flat rotation curve with circular velocity v_c

$$r_c(L) = \frac{L}{v_c}, \tag{A9}$$

$$\Omega(L) = \frac{v_c^2}{L}, \tag{A10}$$

$$\kappa(L) = \sqrt{2}\frac{v_c^2}{L}, \tag{A11}$$

$$E_c(L) = v_c^2 \left(\frac{1}{2} + \ln \frac{L}{L_\odot} \right), \tag{A12}$$

with $L_\odot = R_\odot v_c$.

The difference between energy (equation A1) and that of a circular orbit (equation A12) is related to the orbital eccentricity

$$\frac{E - E_c(L)}{v_c^2} = \frac{\kappa(L) J}{v_c^2} = e^2, \tag{A13}$$

where we have used equations (A3, A8, A11, and A12).

APPENDIX B: DISTANCE DISTRIBUTIONS

In Fig. B1, we show the distribution of distances for the different samples of GALAH stars used to make the histograms shown in Figs 1–6. Stars at all galactic longitudes are included in these histograms. The distribution shows the numbers of stars in 50 pc bins for high-metallicity

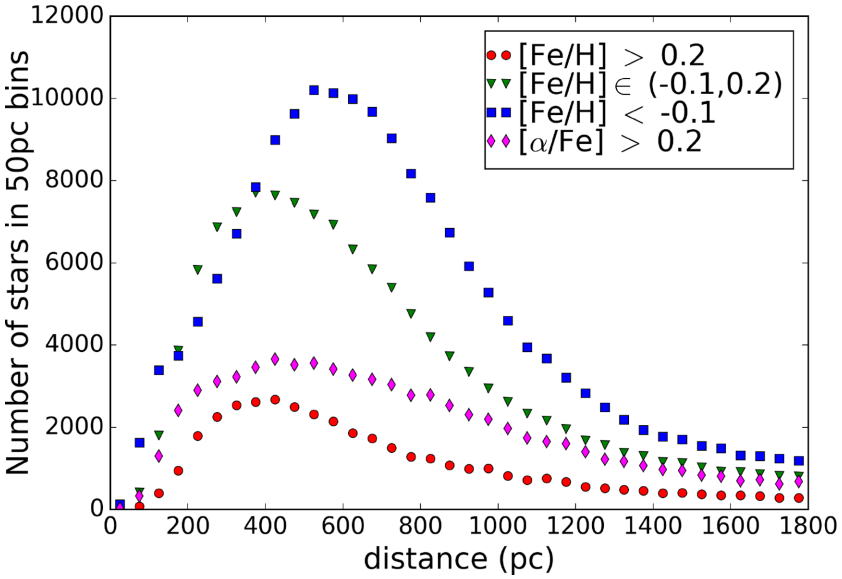

Figure B1. The distribution of distances for the four sets of stars used to construct velocity distributions shown in Figs 1–6.

[Fe/H] > 0.2 (red circles), near solar metallicity −0.1 < [Fe/H] < 0.2 (green triangles), lower metallicity [Fe/H] < −0.1 (blue squares), and high-α-element [α/Fe] > 0.2, and $T_{\rm eff} > 4500^{\circ}$ (magenta diamonds). The distance distributions are consistent with the GALAH sample being dominated by dwarf stars rather than giants.

APPENDIX C: CUTS TO GALAH SURVEY STARS

We list in Table C1 the restrictions and cuts made to the GALAH survey stars when creating figures and tables.

Table C1. List of cuts in the survey data used to make figures and tables.

Description	Restriction	Figures	Tables
High galactic latitude cut	$\|b\| < 45^{\circ}$	All	D1–D4
Fields[a]	$0 <$ field_id ≤ 7338, or field_id ≥ 7357	All	D1–D4
Distance errors	$\sigma_d/d < 0.5$	All	D1–D4
Supersolar metallicities	[Fe/H] > 0.2	Figs 1(a), 2, 3 (top panel),4, 5, 6(a), 7(a), 8–10, 13(a), B1	D1
Near solar metallicities	−0.1 < [Fe/H] < 0.2	Figs 1(b), 2, 6(b), 7(b), 8, 9, 11, 13(b), 14, 15, B1	D2, D4
Subsolar metallicities	[Fe/H] < −0.1	Figs 1(c), 2, 3 (middle panel),6(c), 7(c), 8, 9, 12, 13(c), B1	D3
α-rich	[α/Fe] > 0.2	Figs 1(d), 2, 3 (bottom panel),B1	None
Effective temperature	$T_{\rm eff} > 4500^{\circ}$ K	Figs 1(d), 2, 3 (bottom panel),B1	None
Distance	$0 < d < 500$ pc	Figs 1, 4, 5	None
Distance	$0 < d < 1000$ pc	Figs 2, 3	None
Distance	$0 < d < 250$ pc	Figs 6–15	D1–D4
Northern Galactic hemisphere	$0 < b < 45^{\circ}$	Figs 10(a), 11(a), 12(a), 13 (top panels),14(a), c,15	D4 top
Southern Galactic hemisphere	$0 > b > -45^{\circ}$	Figs 10(b), 11(b), 12(b), 13 (middle panels),14(b), d,15	D4 bottom
M67 field removed[b]	field_id ≠ 6605	Figs 6(b), 7(b), 8, 9, 11, 13(b), 14, 15	D2, D4
Radial velocity component	$-40 < -v_r < 10$ km s^{-1}	Figs 2, 5	None
Galactic longitude	$250^{\circ} < \ell < 290^{\circ}$	Fig. 2	None

Notes. [a]Pilot survey and open cluster target fields are excluded. [b]Stars in the field containing M67 observed as part of the K2-HERMES observing programme are excluded when making histograms of nearby ($d < 250$ pc) and near solar metallicity stars (−0.1 < [Fe/H] < 0.2).

APPENDIX D: VELOCITIES OF PEAKS IN HISTOGRAMS

In Tables D1–D3, we show the (u, v) velocity components of peaks identified in the velocity distributions of Fig. 6 and that are shown in Figs 7–9. Table D1 is for higher metallicity stars, Table D2 is for near solar metallicity stars and Table D3 is for lower metallicity stars. The

Table D1. Peaks in [Fe/H] > 0.2 and $d < 250$ pc (u, v) histograms.

ℓ (°)	u (km s^{-1})	v (km s^{-1})	Height	Stream/group
180	0	0	0.3	
180	−26	−4	0.3	Hyades
180	8	−12	0.2	
200	−28	−8	0.8	Hyades
220	−28	−8	0.7	Hyades
220	14	−8	0.3	Pleiades
240	−10	−10	0.4	Hyades
240	24	−12	0.2	Pleiades
260	−12	−6	0.8	Hyades
260	24	−10	0.4	Wolf630
260	−12	−37	0.4	Hercules
260	14	−43	0.2	HR1614
280	−10	−6	1.3	Hyades
280	−4	−33	0.7	Hercules
280	18	−41	0.4	HR1614
300	26	−6	0.6	Wolf630
300	−10	−4	1.1	Hyades
300	−4	−31	0.6	Hercules
300	20	−39	0.3	HR1614
320	30	−6	0.5	Wolf630
320	−20	−2	0.7	Hyades
320	10	4	0.5	
320	−6	−31	0.4	Hercules
340	−22	−2	0.8	Hyades
340	34	−6	0.5	Wolf630
340	−2	−33	0.3	Hercules
0	−18	−0	0.6	
0	2	4	0.5	
20	−18	−0	0.7	
20	2	4	0.5	

conventions for computing (u, v) (i.e. solar peculiar velocity and LSR circular velocity) are described in Section 2.1. In these tables, galactic longitudes are in degrees and velocities are in km s^{-1}. We have tentatively labelled peaks by their proximity to previously identified moving groups or streams (see Section 5.1). The peaks are identified in histograms that have 4 km s^{-1} square bins in (u, v) and that were smoothed with a Gaussian filter with standard deviation 4 km s^{-1} wide. The precision of these velocity measurements is about ±3 km s^{-1}. The peak height in these tables is in units of numbers of stars in the bin divided by the bin area [16 (km s^{-1})^2] and divided by the number of stars in the histogram.

Table D4 shows (w, v) velocity components of peaks identified in the velocity distributions of Fig. 14 and shown in Fig. 15 for near solar stars metallicity, with $d > 250$ pc, and for stars in the two Galactic hemispheres. Table D4 is similar to Tables D1–D3 except the bins were 3 km s^{-1} wide in v and 1.5 km s^{-1} wide in w. The peak height in this table is in units of numbers of stars in the bin divided by the bin area [4.5 (km s^{-1})^2] and divided by the number of stars in the histogram. The top part of the table shows the northern Galactic hemisphere (latitude $b > 0$) and the bottom half shows the southern Galactic hemisphere.

Table D2. Peaks in $-0.1 < [Fe/H] < 0.2$ and $d < 250$ pc (u, v) histograms.

ℓ (°)	u (km s^{-1})	v (km s^{-1})	Height	Stream/group
180	−4	6	1.2	
180	17	2	0.7	
180	−22	−5	0.9	Hyades
180	−10	−8	1.0	Hyades/Pleiades
200	20	11	0.9	Sirius/UMA
200	−3	4	1.3	Coma Berenices
200	13	−1	0.8	
200	−29	−8	2.4	Hyades
220	19	11	1.0	Sirius/UMA
220	1	4	1.3	Coma Berenices
220	−15	−8	1.4	Pleiades
220	−29	−8	2.4	Hyades
240	18	13	1.2	Sirius/UMA
240	1	2	1.4	Coma Berenices
240	−8	−8	1.3	Hyades
260	20	13	2.2	Sirius/UMA
260	1	4	2.9	Coma Berenices
260	−24	−5	1.7	Hyades
260	−6	−7	2.6	Pleiades
260	−10	−33	0.8	Hercules
280	20	13	2.7	Sirius/UMA
280	3	4	3.3	Coma Berenices
280	−10	−3	3.4	Hyades
280	1	−8	3.2	Pleiades
280	−8	−30	1.2	Hercules
300	20	13	2.4	Sirius/UMA
300	−10	−1	3.4	Hyades
300	3	−7	2.9	Pleiades
300	−10	−30	1.0	Hercules
320	−6	−1	2.6	Hyades/Pleaides
320	17	14	1.8	Sirius/UMA
340	−18	0	2.3	
340	4	4	2.6	
340	24	−3	1.3	
340	−17	−21	1.0	
0	4	2	1.1	
0	−20	4	1.0	
0	18	6	0.7	
0	−10	7	1.0	
0	11	−14	0.6	
20	−19	7	1.2	
20	4	2	1.3	
20	−18	4	1.2	
20	−6	−5	1.2	
40	6	6	0.6	
40	−8	−3	0.5	

Table D3. Peaks in [Fe/H] < -0.2 and $d < 250$ pc (u, v) histograms.

ℓ (°)	u (km s^{-1})	v (km s^{-1})	Height	Stream/group
180	−2	2	1.4	
180	−20	−4	1.1	Hyades
200	14	10	1.2	Sirius/UMA
200	−4	2	1.4	Coma Berenices
200	−22	−8	1.4	Hyades
220	18	10	1.1	Sirius/UMA
220	−6	2	1.1	Coma Berenices
220	−20	−10	1.4	Hyades
240	14	12	1.0	Sirius/UMA
240	−2	2	0.9	Coma Berenices
240	−16	−8	1.0	Hyades
240	4	−8	1.0	Pleiades
260	12	14	2.3	Sirius/UMA
260	0	0	2.3	Coma Berenices
260	4	−12	2.3	Pleiades
280	2	2	3.4	
300	6	−4	3.5	
320	8	−4	3.0	
340	6	0	2.7	
340	−10	6	2.3	
0	−2	6	1.2	
20	0	6	1.3	
40	18	18	0.5	

Table D4. Peaks in $-0.1 <$ [Fe/H] < 0.2 and $d < 250$ pc (w, v) histograms with Galactic hemisphere.

ℓ (°)	w (km s^{-1})	v (km s^{-1})	Height	Stream/group
For Galactic latitude $b > 0$				
200	−4.5	14.5	0.4	Sirius/UMa
200	−2.2	−9.5	1.2	Hyades/Pleiades
220	−1.5	11.5	0.5	Sirius/UMa
220	5.2	−8.0	1.1	
220	−1.5	−8.0	1.3	Hyades/Pleiades
240	0.8	13	0.5	Sirius/UMa
240	0.0	−8.0	0.5	
240	4.5	−9.5	0.6	Hyades/Pleiades
260	1.5	11.5	0.6	Sirius/UMa
260	−4.5	−0.5	0.6	
260	4.5	−8.0	1.1	Hyades/Pleiades
280	2.2	14.5	0.6	Sirius/UMa
280	−6.0	−5.0	0.8	
280	3.8	−8.0	1.3	Hyades/Pleiades
300	2.2	13.0	0.8	Sirius/UMa
300	2.2	−0.5	1.5	
320	3.0	−2.0	1.6	
340	3.0	1.0	1.7	
0	3.0	1.0	0.6	
20	0.0	4.0	0.7	
20	3.0	1.0	0.7	
For Galactic latitude $b < 0$				
180	−1.5	4.0	1.2	Coma Berenices
180	−4.5	−5.0	1.0	
200	−1.5	5.5	0.8	Coma Berenices
200	0.8	−12.5	0.6	Hyades/Pleiades
220	−1.7	2.5	0.6	Coma Berenices
220	1.0	−12.5	0.6	Hyades/Pleiades
240	−3.0	2.5	0.8	Coma Berenices
240	1.5	−12.5	0.6	Hyades/Pleiades
260	−3.8	4.0	1.6	Coma Berenices
260	1.8	−7.3	1.3	Hyades/Pleiades
280	−3.8	4.0	1.6	Coma Berenices
280	1.5	−6.5	2.0	
300	−3.8	4.0	1.3	
300	0.8	−3.5	1.5	
320	−3.8	8.5	0.9	
320	3.8	5.5	1.0	
320	0.0	−3.5	1.1	
340	−3.8	8.5	0.9	
340	0.8	−5.0	0.9	
0	1.5	4.0	0.7	
0	4.5	−8.0	0.6	
20	1.5	5.5	0.7	
20	5.2	−5.0	0.6	
40	5.0	2.5	0.4	

[1]*Department of Physics and Astronomy, University of Rochester, Rochester, NY 14627, USA*
[2]*Australian Astronomical Observatory, 105 Delhi Rd, North Ryde, NSW 2113, Australia*
[3]*Sydney Institute for Astronomy, School of Physics, A28, The University of Sydney, Sydney NSW 2006, Australia*
[4]*Australian Research Council Centre of Excellence for All Sky Astrophysics in 3 Dimensions (ASTRO-3D), Canberra, ACT 72611, Australia*
[5]*Research School of Astronomy and Astrophysics, Australian National University, Cotter Road, Canberra, ACT 72611, Australia*
[6]*Miller Professor, Department of Astronomy, Campbell Hall, UC Berkeley, CA 94720, USA*
[7]*Max-Planck-Institut for Astronomy, Königstuhl 17, D-69117 Heidelberg, Germany*
[8]*Istituto Nazionale di Astrofisica, Osservatorio Astronomico di Padova, vicolo dell'Osservatorio 5, I-35122 Padova, Italy*
[9]*Department of Physics and Astronomy, Uppsala University, Box 516, SE-751 20 Uppsala, Sweden*
[10]*School of Physics, University of New South Wales, Sydney, NSW 2052, Australia*
[11]*Department of Physics and Astronomy, Macquarie University, Sydney, NSW 2109, Australia*
[12]*Research Centre in Astronomy, Astrophysics & Astrophotonics, Macquarie University, Sydney, NSW 2109, Australia*
[13]*Faculty of Mathematics and Physics, University of Ljubljana, Jadranska 19, 1000 Ljubljana, Slovenia*
[14]*Department of Astronomy, University of Virginia, PO Box 400325, Charlottesville, VA 22904, USA*

[15] *Istituto Nazionale di Astrofisica, Via dell'Osservatorio 20, Pino Torinese I-10025, Italy*
[16] *School of Physical and Chemical Sciences, University of Canterbury, Christchurch 8140, New Zealand*
[17] *Monash Centre for Astrophysics, School of Physics and Astronomy, Monash University, Clayton 3800, Victoria, Australia*
[18] *ICRAR, The University of Western Australia, 35 Stirling Highway, Crawley, WA 6009, Australia*
[19] *Division of Research and Innovation, University of Southern Queensland, Toowoomba, Queensland 4350, Australia*
[20] *Center for Astrophysical Sciences and Department of Physics and Astronomy, The Johns Hopkins University, Baltimore, MD 21218, USA*
[21] *Institute for Advanced Study, Princeton, NJ 08540, USA*
[22] *Department of Astrophysical Sciences, Princeton University, Princeton, NJ 08544, USA*
[23] *Observatories of the Carnegie Institution of Washington, 813 Santa Barbara Street, Pasadena, CA 91101, USA*
[24] *University of Southern Queensland, Computational Engineering and Science Research Centre, Toowoomba, Queensland 4350, Australia*
[25] *Australian Centre for Astrobiology, University of New South Wales, Sydney, NSW 2052, Australia*

This paper has been typeset from a TEX/LATEX file prepared by the author.